공학박사 학위논문

IMPROVING DOA ESTIMATION USING VIRTUAL ANTENNA IN AUTOMOTIVE RADAR

차량용 레이더를 위한 가상 안테나를

이용한 각도 추정 성능 개선

2017년 2월

서울대학교 대학원

전기·컴퓨터 공학부

강석현

IMPROVING DOA ESTIMATION USING VIRTUAL ANTENNA IN AUTOMOTIVE RADAR

지도 교수 김 성 철

이 논문을 공학박사 학위논문으로 제출함

2017년 2월

서울대학교 대학원

전기·컴퓨터 공학부

강 석 현

강석현의 공학박사 학위논문을 인준함

2017년 2월

위 원 장 조 남 익 (인)

부위원장 김 성 철 (인)

위 원 김 남 수 (인)

위 원 김 영 록 (인)

위 원 정 성 희 (인)

Abstract

IMPROVING DOA ESTIMATION USING VIRTUAL ANTENNA IN AUTOMOTIVE RADAR

Seokhyun Kang
Department of Electrical and Computer Engineering
The Graduate School
Seoul National University

These days, drivers regard safety as the most important issue in vehicular technology. This fact has led to the development of several types of sensors that help increase driver and vehicle awareness of the circumstances around a car. Such automotive sensor include cameras and ultrasonic and radar sensor. Among these sensors, radar sensors are most widely used because of their dependability in a variety of environmental conditions. The FMCW radar in

77 GHz has widely being studied for the reason of considering about global environment. Previous automotive radar systems are simply to obtain information about the distance between the observer and the target and the velocity of both. However, as safety consciousness has become more important to drivers, the use of radar systems has developed dramatically.

The DOA estimation algorithms have been recognized for their usefulness for determining the degree of targets using digital beamforming techniques. MUSIC, Root-MUSIC, and ESPIRIT, the high resolution DOA estimation algorithms, are used to distinguish very adjacent objects. Through these algorithms, it is possible to obtain information about delay time and frequency as well as degree. These algorithms have recently been investigated regarding their application towards enhancing the function of practical automotive radars. The information obtained from DOA estimation algorithms is being applied to a variety of uses, such as the cancellation of interference between signals, and the removal of cluster resulting from undesired objects.

In this dissertation, the virtual antenna technique is applied to a single input multiple output (SIMO) radar system to enhance the performance of the conventional beamforming direction of arrival (DOA) estimation method. Combining the virtual array generated by the interpolated array technique and the real array, the angular resolution of the DOA estimation algorithm is

improved owing to the extended number of antennas and aperture size. Based on the proposed interpolation technique, we transform the position of the antenna elements in a uniform linear array (ULA) to the arbitrary positions to suppress the grating lobe and side lobe levels. In simulations, the pseudo spectrum of the Bartlett algorithm and the root mean square error (RMSE) of the DOA estimation with the signal-to-noise ratio (SNR) are analyzed for the real array and the proposed virtually extended array. Simulation results show that the angular resolution of the proposed array is better than that of the real array using the same aperture size of array and the number of antennas.

Keywords : FMCW, Automotive radar, Direction Of Arrival(DOA), Interpolated array, Virtual antenna

Student Number : 2010 - 23241

Contents

List of Tables

List of Figures

Chapter 1. Introduction

The most important issue in the vehicular technology is preventing accidents. This fact has led to the development of several types of sensors that help drivers to aware the circumstances around vehicles. For examples, cameras, ultrasonic and radar sensor are included in the automotive sensors. The radar sensor is most widely used among these sensors, because of its independence from a variety of environmental conditions.

The purpose of automotive radar is to give the safety to drivers and pedestrians from unexpected accident in various traffic situations. The system for this purpose is called driver assistance system (DAS). Many automobile device companies have already developed many kinds of DASs such as adaptive cruise control (ACC), forward collision warning (FCW), pre-crash safety (PCS), blind spot detection (BSD), lane change assist (LCA) and rear cross traffic alert application (RCTA) system. ACC system is a radar-based system that can detect the vehicles in front, and adjust speed of the vehicles to keep a pre-set following distance, even under fog and rain conditions. FCW system is in-vehicle electronic that monitor the roadway in front of the host vehicle and warn the driver when a potential collision risk exists. When the sign of collision is detected, it provides a red light that flashes on the

windshield. PCS is system that detects the potential collision using the sensor and activates all necessary component such as brakes, airbag or steering in the car to avoid an accident. The vehicles on adjacent lanes can be avoided by BSD system which is invisibly mounted in the corners of the rear bumper. Also, the field of view for LCA system is selected to cover most of the blind spot warning zone and area containing neighbor lanes. An acoustic warning for drivers from BSD sensor would be helpful in a critical situation. RCTA system can assist drivers in backing up by warning drivers of impending traffic while reversing.

The 77 GHz frequency modulated continuous wave (FMCW) radar has been widely studied in these days. The system is used not only for obtaining the range and the velocity of targets, but also for measuring the angular position of the targets. The direction of arrival (DOA) estimation algorithms such as the conventional beamforming (i.e., the Bartlett estimation), the multiple signal classification (MUSIC), the Root-MUSIC, and the estimation of parameters via rotational invariance technique (ESPRIT) have been equipped with the FMCW radar system for determining the angle information of the desired targets [1]-[3]. These algorithms can be allowed with certain conditions for the number of desired targets, incoherence of received signals reflected from different targets, and the angular location of targets, etc. [4], [5].

When the assumptions on the prior information are satisfied, most of these algorithms show superior performance. However, it is hard to fulfill the assumptions on the prior information in the practical situation. The performance of the MUSIC algorithm, known as the super-resolution DOA estimation algorithm, is even worse than the performance for the more robust conventional DOA estimation algorithm (e.g. the Bartlett estimation). For example, the MUSIC algorithm operates properly when the signals reflected from different targets are incoherent and the number of targets is perfectly known. Since the algorithm is applied for the practical case where the signals could be coherent and the number of targets is veiled, the prior assumption may not be valid for the FMCW radar systems.

Of late, improving the performance of radar and cutting down production cost is a critical issue for automotive radar. As the number of arrays decrease, the production cost also decrease. To make the size of radar smaller, the concept of virtual antenna array is devised in order to get the same performance with fewer antennas than previously. The concept is generally applied to the MIMO radar in ULA but a practical automotive radar consists of one transmit antenna.

In this dissertation, the virtual antenna array concept was applied to the single transmit antenna system for automotive radar to distinguish the closely

adjacent targets. The angular resolution can be enhanced by extending the aperture size of array and expanding the number of antennas. Therefore, I propose a virtual antenna generated by the interpolated array technique to increase the angular resolution while maintaining the given aperture size of the array and the number of antennas [6]-[11]. Since the proposed technique provides an enhanced angular resolution without increasing the aperture size of the array and the number of antennas, it enables to design the compact radar. The performance of the proposed virtual array is almost equivalent to the DOA estimation performance of the large aperture size of the array and the more number of antennas.

Chapter 2. Analysis of High Resolution DOA Estimation Algorithm

2.1 Introduction

Array signal processing has wide applications, such as radar, sonar, medicine, earthquake, satellite, and communication system. It becomes a hotspot and difficult point in the signal processing domain. Array signal processing aims at processing signals received by array antenna, strengthening useful signals, restraining the interference and noise, while at the same time collecting useful signal parameters. Compared with traditional signal orientation sensor, sensor array can control the beam flexibly, with a high signal gain and strong ability for interference. That is the reason why array signal processing theory can boom in recent decade.

Signal processing in smart antenna systems concentrates on the development of efficient algorithms for Direction of Arrival (DOA) estimation and adaptive beam forming. However, there are many limitations if DOA estimation uses a fixed antenna. Antenna main-lobe beam width is inversely proportional to its physical shape. It is not a practical option to

improve the accuracy of angle measurement in accordance with an increase in the physical aperture of the receiving antenna. Some systems such as missile seeker or aircraft antenna have limited physical size, so they are sufficiently wide in beam width of the main lobe to correspond. They do not have a good resolution and if there are multiple signals falling in the antenna's main lobe, it becomes too difficult to distinguish between them. Using an array antenna system with innovative signal processing instead of a single antenna can enhance the resolution of the DOA estimation. This array structure provides spatial samplings of the received waveform. In signal reception and parameter estimation, a sensor array has better performance than a single sensor.

There are many kinds of super resolution algorithms such as spectral estimation, Bartlett, Capon, ESPRIT, Min-norm and MUSIC. One of the most popular and widely used subspace-based techniques to estimate the DOA of multiple signal sources is the MUSIC algorithm. Large numbers of computations are needed to search for the spectral angle when using the MUSIC algorithm, so in real applications its implementation can be difficult. Compared with spectral MUSIC algorithm, the Root-MUSIC method has better performance with reduced complexity computation.

2.2 Data Model

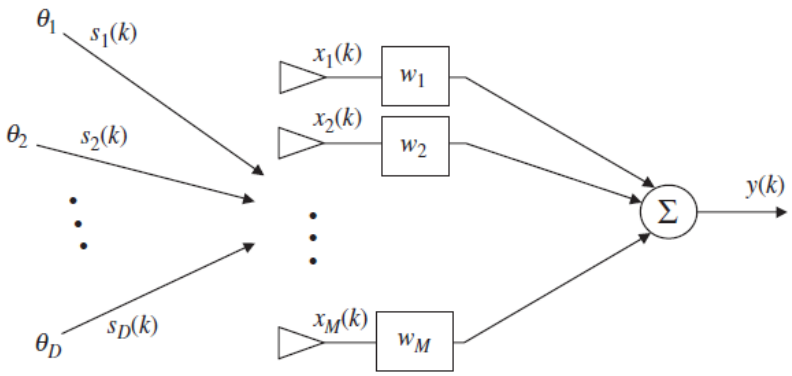

Figure 2.1. The system structure of DOA estimation

There are D targets and M uniform linear array. The array output at the *k*-th time sample can be modeled as,

$$y(k) = \bar{w}^T \cdot \bar{x}(k) \tag{2.1}$$

where $\bar{\mathrm{w}} = [w_1 \; w_2 \cdots w_M]^T$ are array weights. And, the received signal $\bar{x}(k)$ is formulated as,

$$\begin{aligned} \bar{x}(k) &= [\bar{a}(\theta_1) \; \bar{a}(\theta_2) \; \cdots \; \bar{a}(\theta_D)] \cdot \begin{bmatrix} s_1(k) \\ s_2(k) \\ \vdots \\ s_D(k) \end{bmatrix} + \bar{n}(k) \\ &= \mathbf{A}(k) \cdot \bar{s}(k) + \bar{n}(k) \end{aligned} \tag{2.2}$$

where $\mathbf{A} = [a(\theta_1), a(\theta_2), \cdots, a(\theta_D)]$ is the steering matrix, $\mathbf{a}(\theta) = [1 \;\; e^{jkd\sin\theta} \;\; e^{j2kd\sin\theta} \cdots \; e^{j(M-1)kd\sin\theta}]^T (M \times 1)$ is the steering vector for the DOA, $\overline{s}(k)$ is the incident signal vector at time k, and $\overline{n}(k)$ denotes the noise vector at each array element with white Gaussian noise.

Array correlation matrix is expressed as,

$$\begin{aligned}\overline{\mathbf{R}}_{xx} &= E[\overline{x} \cdot \overline{x}^H] - (E[\overline{x}])^2 \\ &= E[(\mathbf{A}\overline{s} + \overline{n})(\overline{s}^H \mathbf{A}^H + \overline{n}^H)] - (E[\mathbf{A}\overline{s} + \overline{n}])^2 \\ &= \mathbf{A}E[\overline{s} \cdot \overline{s}^H]\mathbf{A}^H + E[\overline{n} \cdot \overline{n}^H] \\ &= \mathbf{A}\overline{R}_{ss}\mathbf{A}^H + \overline{R}_{nn}\end{aligned} \tag{2.3}$$

The eigenvalue decomposition of its correlation matrix is

$$\overline{\mathbf{R}}_{xx} = \mathbf{A}\overline{\mathbf{R}}_{ss}\mathbf{A}^{\mathbf{H}} + \sigma^2\mathbf{I} = \mathbf{U_s}\mathbf{\Lambda_s}\mathbf{U_s^H} + \mathbf{U_n}\mathbf{\Lambda_n}\mathbf{U_n^H} \tag{2.4}$$

Where $\overline{\mathbf{R}}_{ss} = E[\overline{s}(k) \cdot \overline{s}^H(k)]$ is the signal correlation matrix, $\mathbf{I}$ is the identity matrix, $\mathbf{U_s}$ are the eigenvectors of the signal subspace of D dimension and $\mathbf{U_n}$ are the M-D dimensional eigenvectors with the noise subspace.

If we don't know the exact statistics for the noise and signals, but we can assume that the process is ergodic, then we can approximate the correlation by

use of a time averaged correlation. In that case the correlation matrices are defined by,

$$\hat{\mathbf{R}}_{xx} \approx \frac{1}{K}\sum_{k=1}^{K} \overline{x}(k)\cdot \overline{x}^{H}(k) \quad \hat{\mathbf{R}}_{ss} \approx \frac{1}{K}\sum_{k=1}^{K} \overline{s}(k)\cdot \overline{s}^{H}(k) \tag{2.5}$$

2.3 Bartlett Algorithm

The conventional beamformer technique developed by Bartlett is considered to be one of the oldest techniques for DOA estimation for signal sources. Beamformer steers the array in one direction at a time and measures the output power. The direction which gives maximum output power provides the true DOA for the incident sources[1]-[3].

The array output is formed by a linear combination of the antenna outputs with a weighting factor

$$y(k) = \mathbf{w}^{H}\mathbf{x}(k) \tag{2.6}$$

Maximizing the output power is formulated as,

$$
\begin{aligned}
p(w) &= \max_{w} E[\left|y(k)\right|^2] = \max_{w} E[\mathbf{w}^H \mathbf{x}(k)\mathbf{x}^H(k)\mathbf{w}] \\
&= \max_{w} \mathbf{w}^H E[\mathbf{x}(k)\mathbf{x}^H(k)]\mathbf{w} \\
&= \max_{w} \{E[\left|\mathbf{s}(k)\right|^2]\left|\mathbf{w}^H a(\theta)\right|^2 + \sigma^2 \left|\mathbf{w}\right|^2\}
\end{aligned}
\tag{2.7}
$$

To obtain a solution, the norm of w is constrained to $|w| = 1$ when carrying out the maximization.

The resulting solution is given by,

$$
\mathbf{w} = \frac{\mathbf{a}(\theta)}{\sqrt{\mathbf{a}^H(\theta)\mathbf{a}(\theta)}} \tag{2.8}
$$

The $M \times 1$ weight vector can be interpreted as a spatial filter, which has been matched to the impinging signals. Applying the weighting vector into Eq. (2.7), the Bartlett pseudo-spectrum is obtained [1].

$$
P_B(\theta) = \frac{\mathbf{a}^H(\theta)\hat{\mathbf{R}}_{xx}\mathbf{a}(\theta)}{\mathbf{a}^H(\theta)\mathbf{a}(\theta)} \tag{2.9}
$$

To analysis the performance of Bartlett algorithm, 8 uniform linear arrays with 0.5λ antenna spacing, 10dB SNR, 100 time samples are used. 100 simulation trials using two targets located at [0º, 20º], [0º, 10º].

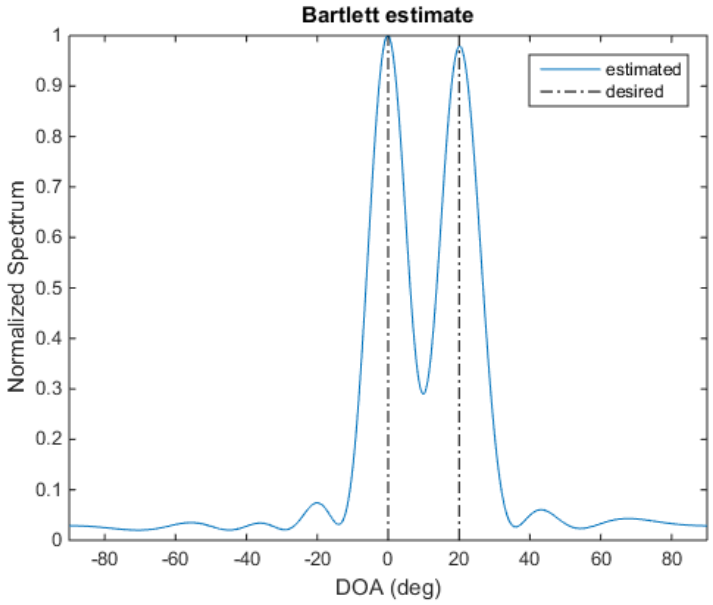

Figure 2.2 Bartlett spectrum with [0º, 20º]

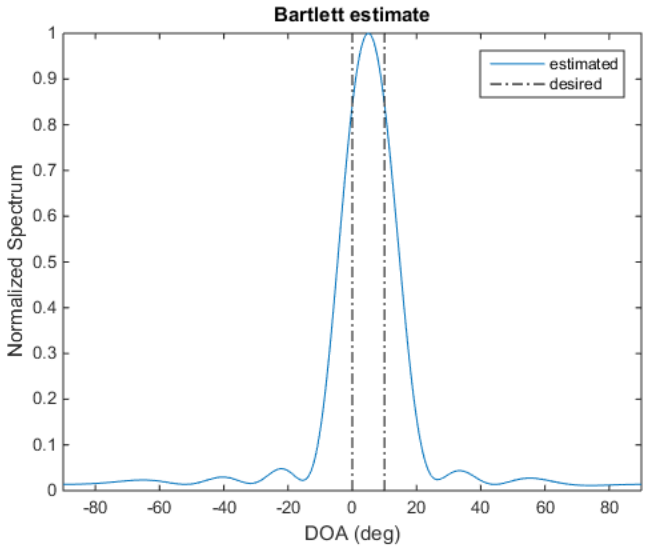

Figure 2.3 Bartlett spectrum with [0º, 10º]

In the second case, target is fixed at [0º, 10º] and SNR is varied.

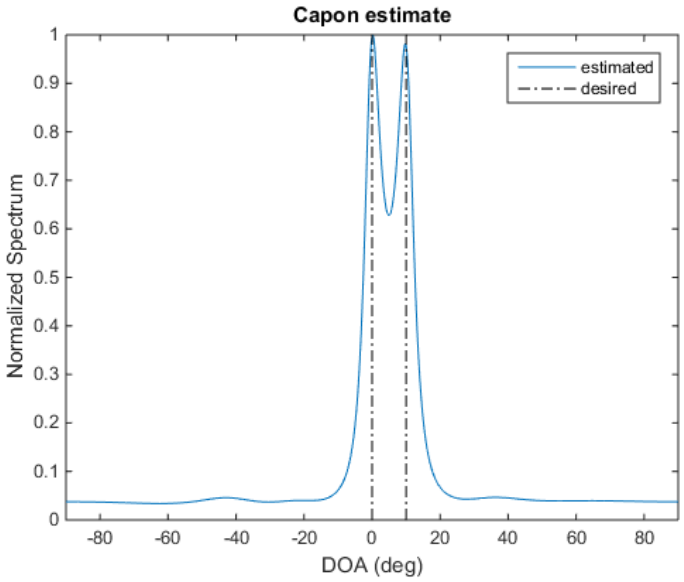

Figure 2.4 Bartlett spectrum with 5dB SNR

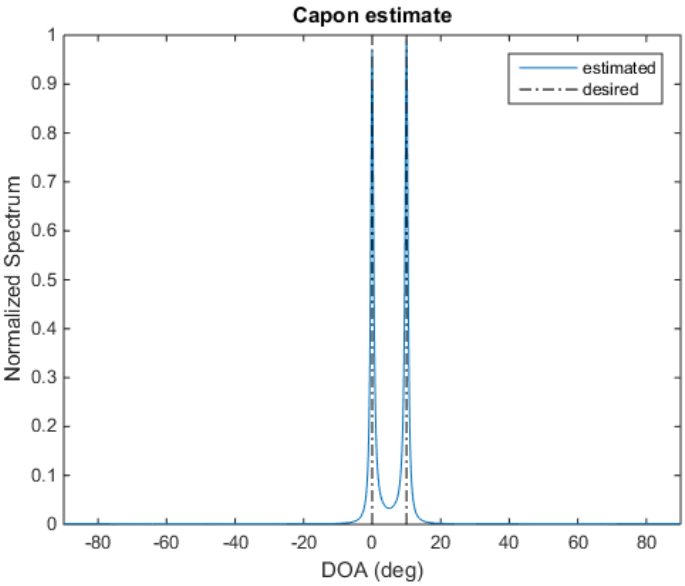

Figure 2.5 Bartlett spectrum with 20dB SNR

2.4 Capon Algorithm

The capon algorithm is known as a minimum variance distortionless response (MVDR). It is also alternatively a maximum likelihood estimate of the power arriving from one direction while all other sources are considered as interference. Thus, the goal is to maximize the signal-to-intereference ratio (SIR) while passing the signal of interest undistorted in phase and amplitude. This property will limit the resolutions for the conventional beamformer. Capon proposed to minimize the contribution of undesired DOAs by minimizing the total output power while maintaining the gain along the look direction as constant.

$$\min_{\mathbf{w}}(w^H \bar{R} w) \quad subject\ to\ \left|w^H a(\theta)\right| = 1 \tag{2.10}$$

For a positive definite correlation matrix, the solution of equation (2.10) of the weight vector can be given by,

$$\bar{w} = \frac{\hat{R}^{-1} a(\theta)}{a(\theta)^H \hat{R}^{-1} a(\theta)} \tag{2.11}$$

The weight obtained by equation (2.11) is called MVDR. With this weight vector in equation (2.10), the array output signal power has the form,

$$P_C(\theta) = \frac{a(\theta)^H a(\theta)}{a(\theta)^H \hat{R}^{-1} a(\theta)} \tag{2.12}$$

where the DOAs can be found from the *D* highest peak of the spatial spectrum of equation (2.12). Capon's method gives better performance than the conventional beamformer. However, Capon still depends on the number of elements array and on the SNR. Also, it is not able to resolve the DOAs for correlated sources.

To analysis the performance of Capon algorithm, 8 uniform linear arrays with 0.5λ antenna spacing, 10dB SNR, 100 time samples are used. 100 simulation trials using two targets located at [0º, 10º], [0º, 5º].

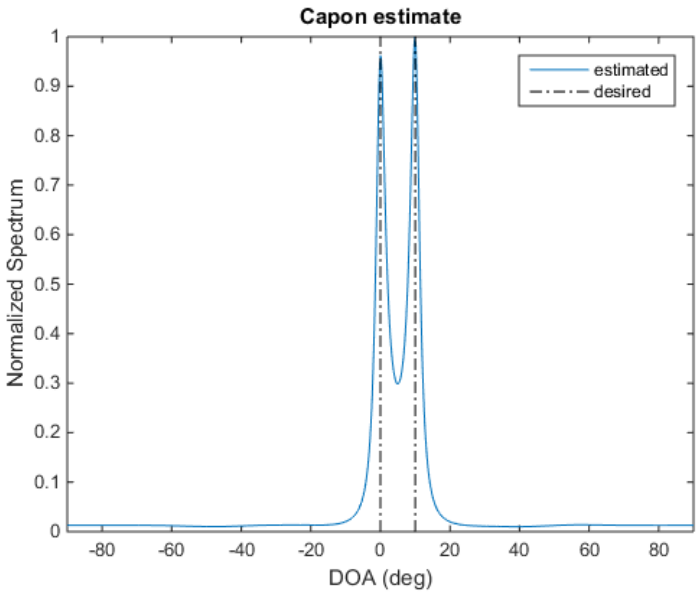

Figure 2.6 Capon spectrum with [0º, 10º]

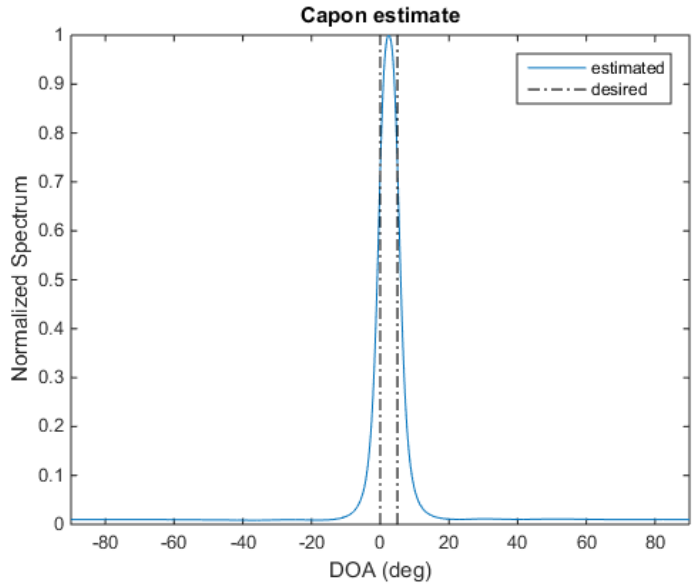

Figure 2.7 Capon spectrum with [0º, 5º]

In the second case, target is fixed at [0º, 10º] and SNR is varied.

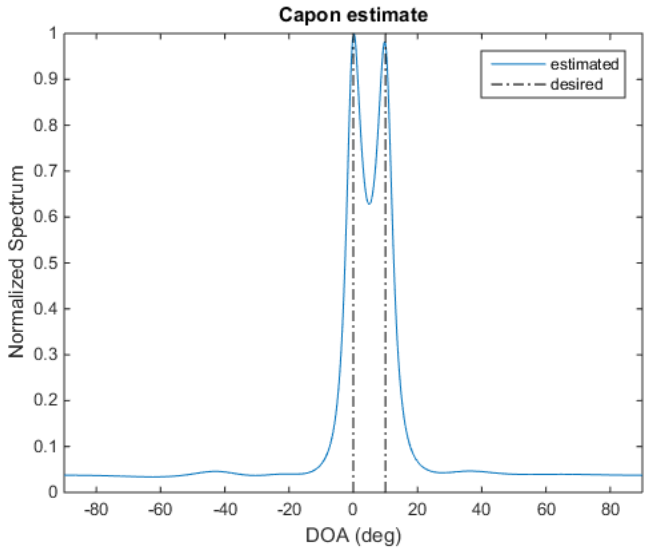

Figure 2.8 Capon spectrum with 5dB SNR

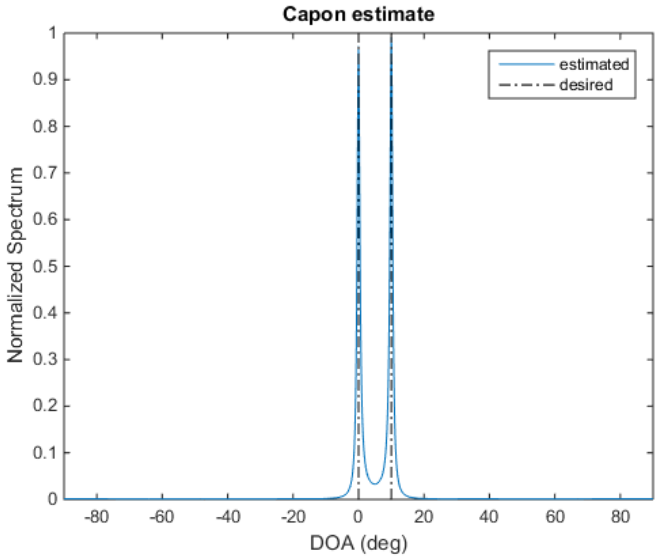

Figure 2.9 Capon spectrum with 20dB SNR

2.5 MUSIC Algorithm

MUSIC is an acronym which stands for MUltiple SIgnal Classification. This approach was first posed by Schmidt [1] and is a popular high resolution eigenstructure method. MUSIC promises to provide unbiased estimates of the number of signals, the angles of arrival, and the strengths of the waveforms. MUSIC makes the assumption that the noise in each channel is uncorrelated making the noise correlation matrix diagonal. The incident signals may be somewhat correlated creating a non-diagonal signal correlation matrix. However, under high signal correlation the traditional MUSIC algorithm breaks down and other methods must be implemented to correct this weakness. These methods will be discussed later in this chapter. One must know in advance the number of incoming signals or one must search the eigenvalues to determine the number of incoming signals.

The eigenvalues of the matrix $\bar{R}_{xx}$ are sorted in accordance with size, which is,

$$\lambda_1 \geq \lambda_2 \geq \cdots \geq \lambda_M > 0 \tag{2.13}$$

where larger eigenvalues D are corresponding to signal while M-D smaller eigenvalues are corresponding to noise.

The eigenvalues and eigenvectors which belong to matrix $\bar{R}_{xx}$ are corresponding to signal and noise respectively. Therefore, the eigenvalue (eigenvector) of $\bar{R}_{xx}$ to signal eigenvalue (eigenvector) and noise eigenvalue (eigenvector) can be divided.

We can then construct the $M \times (M - D)$ dimensional subspace spanned by the noise eigenvectors such that

$$\bar{E}_N = [\bar{e}_1 \ \bar{e}_2 \ \cdots \ \bar{e}_{M-D}] \tag{2.14}$$

The noise subspace eigenvectors are orthogonal to the array steering vectors at the angles of arrival $\theta_1, \theta_2, \cdots, \theta_D$. Because of this orthogonality condition, one can show that the Euclidean distance $d^2 = \left|\bar{a}^H(\theta)\bar{E}_N\bar{E}_N^H\bar{a}(\theta)\right| = 0$ for each and every arrival angle $\theta_1, \theta_2, \cdots, \theta_D$. Placing this distance expression in the denominator creates sharp peaks at the angles of arrival. The MUSIC pseudospectrum is now given as

$$P_{MUSIC}(\theta) = \frac{1}{\left|\bar{a}^H(\theta)\bar{E}_N\bar{E}_N^H\bar{a}(\theta)\right|} \tag{2.15}$$

To analysis the performance of MUSIC algorithm, 8 uniform linear arrays with 0.5λ antenna spacing, 10dB SNR, 100 time samples are used. 100 simulation trials using two targets located at [0º, 5º].

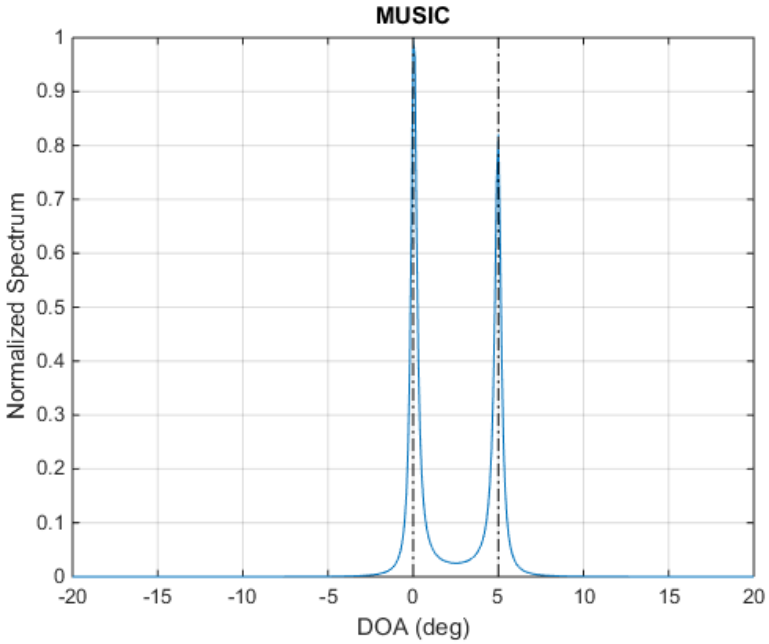

Figure 2.10 MUSIC spectrum with [0º, 5º]

2.6 Root−MUSIC Algorithm

The MUSIC algorithm in general can apply to any arbitrary array regardless of the position of the array elements. Root-MUSIC implies that the MUSIC algorithm is reduced to finding roots of a polynomial as opposed to merely plotting the pseudospectrum or searching for peaks in the pseudospectrum. Barabell [1] simplified the MUSIC algorithm for the case where the antenna is a ULA. Recalling that the MUSIC pseudospectrum is given by,

$$P_{MUSIC}(\theta) = \frac{1}{\left|\overline{a}^{H}(\theta)\overline{E}_{N}\overline{E}_{N}^{H}\overline{a}(\theta)\right|} \tag{2.16}$$

In equation (2.16), the denominator can be simplified by defining the matrix as $C = \overline{E}_{N}\overline{E}_{N}^{H}$. This leads to the Root-MUSIC spectrum is given by,

$$P_{R-MUSIC}(\theta) = \frac{1}{\left|\overline{a}^{H}(\theta)C\overline{a}(\theta)\right|} \tag{2.17}$$

The denominator of equation (2.17) can be written as,

$$\begin{aligned}\overline{a}^{H}(\theta)C\overline{a}(\theta) &= \sum_{m=1}^{M}\sum_{n=1}^{M} e^{-jkd(m-1)\sin\theta} C_{mn} e^{jkd(n-1)\sin\theta} \\ &= \sum_{l=-M+1}^{M-1} c_{l} e^{jkdl\sin\theta}\end{aligned} \tag{2.18}$$

where c_l is the sum of the diagonal elements of matrix C. Let define $z = e^{jkd\sin\theta}$, equation (2.18) can be simplified as the form of a polynomial with coefficient c_l.

$$D(z) = \sum_{l=-N+1}^{N-1} c_l z^l = 0 \tag{2.19}$$

Among the roots of the polynomial $D(z)$ within the unit circle, choose the D closest to the unit circle correspond to the poles of the pseudo-spectrum. The phase angle of the each root implies the angle of the targets.

$$\theta_i = -\sin^{-1}\left(\frac{1}{kd}\arg(z_i)\right), \quad i = 1, \cdots, D \tag{2.20}$$

With 8 elements of array, 10 dB SNR, and two targets located at [0º, 5º], there are 14 roots in the Cartesian coordinates in figure 2.11. I can choose the two roots closest to the unit circle and replot them along with the MUSIC spectrum in figure 2.12.

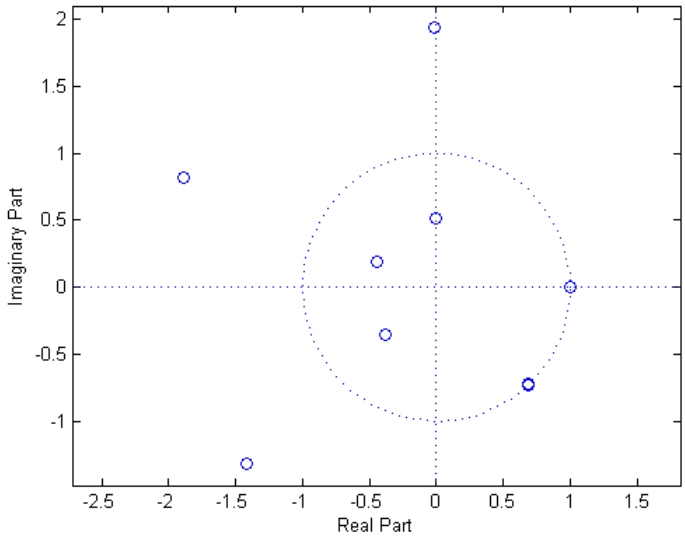

Figure 2.11 Roots in Cartesian coordinates

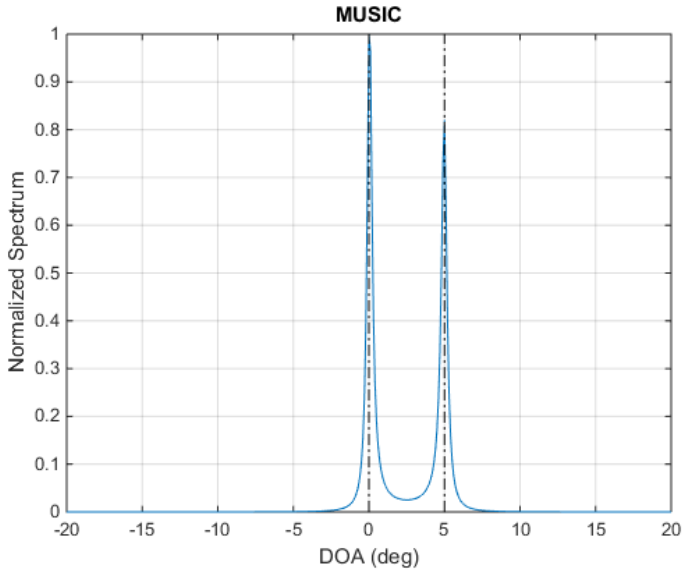

Figure 2.12 MUSIC spectrum and roots found with root-MUSIC

2.7 ESPRIT Algorithm

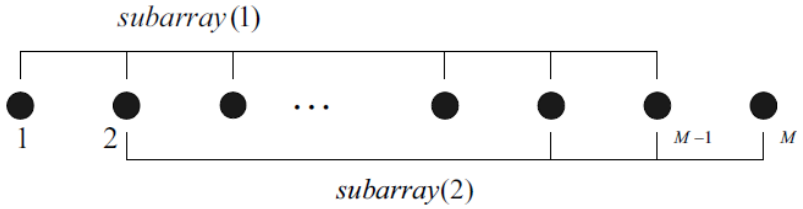

Figure 2.13 The system structure of ESPRIT

ESPRIT represents Estimation of Signal Parameters via Rotational Invariance Techniques. This algorithm is more robust with respect to computational complexity than MUSIC because it does not use the peak detection of all possible steering vectors. ESPRIT is based on multiple identical arrays called “doublets”. The array elements are placed in identical displacement translationally but not rotationally. The two subarrays are displaced by distance *d*. Let us call these arrays array 1 and array 2. The received signal for array 1 is,

$$x_1(k) = A_1 s(k) + n_1(k) \tag{2.21}$$

and, for array 2 is

$$\begin{aligned} x_2(k) &= A_2 s(k) + n_2(k) \\ &= A_1 \Phi s(k) + n_2(k) \end{aligned} \tag{2.22}$$

where $L \times L$ unitary matrix Φ

$$\Phi = diag[e^{jkd\sin\theta_1}, e^{jkd\sin\theta_2}, \cdots, e^{jkd\sin\theta_D}] \tag{2.23}$$

Assuing the two subarrays of the signal subspace possess eigenvectors $\overline{E}_{s1}$ and $\overline{E}_{s2}$, both $\overline{E}_{s1}$ and $\overline{E}_{s2}$ are $N \times L$ matrices corresponding to the largest eigenvalues of the correlation matrix of each subarray. Since the two subarrays are translationally displaced, the eigenvectors of the two subarrays are related by a unique non-singular transformation matrix $\boldsymbol{\varphi}$ where,

$$\overline{E}_{s1}\boldsymbol{\varphi} = \overline{E}_{s2} \tag{2.24}$$

There should exist a non-singular transformation matrix $\mathbf{T}$ such that,

$$\boldsymbol{\varphi} = \mathbf{T}^{-1}\boldsymbol{\Phi}\mathbf{T} \tag{2.25}$$

If the eigenvalues of $\boldsymbol{\varphi}$ ($\lambda_1, \lambda_2, \cdots, \lambda_L$) are found, the DOA can be estimated as,

$$\theta_i = \sin^{-1}\left(\frac{\arg(\lambda_i)}{kd}\right), \quad i = 1, 2, \cdots, D \tag{2.26}$$

2.8 Simulation Results

To compare the performance of different DOA algorithms, the RMSE of each algorithm is analyzed using MATLAB. Generally, 8 uniform linear arrays with 0.5λ antenna spacing are used. The signals were generated with random phases to produce uncorrelated signals.

Figure 2.14, 2.15 shows the RMSE via SNR (0dB~20dB) of 100 simulation trials using two targets located at [10º, 25º]. As the SNR increases, the RMSE becomes smaller increasing the accuracy of the algorithm.

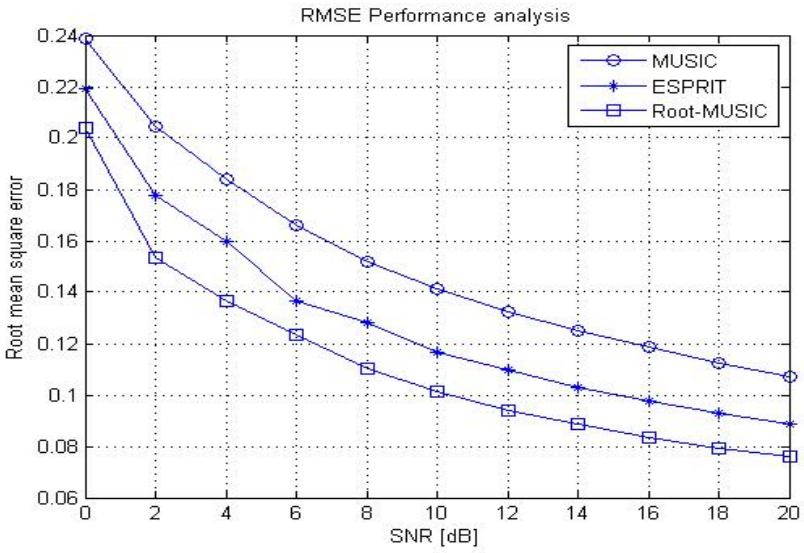

Figure 2.14 RMSE performances for [10º, 25º] with 200 time samples

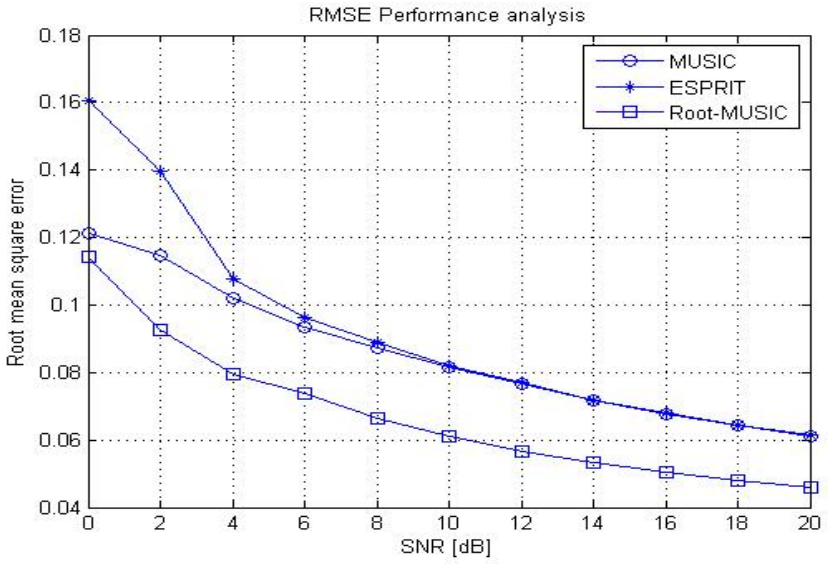

Figure 2.15 RMSE performances for [10º, 25º] with 500 time samples

When the number of time sample is 200, the RMSE performance of ESPRIT algorithm is better than that of MUSIC algorithm. However, when the number of time sample is increased, the better RMSE performance shows in the MUSIC algorithm. It means that the performance of MUSIC algorithm is influenced by the number of time sample.

Chapter 3. The Grating Lobe Suppression Technique

3.1 Introduction

The most important issue in the vehicular technology is preventing accidents. This fact has led to the development of several types of sensors that help drivers to aware the circumstances around vehicles. For examples, cameras, ultrasonic and radar sensor are included in the automotive sensors. The radar sensor is most widely used among these sensors, because of its independence from a variety of environmental conditions.

The 77 GHz frequency modulated continuous wave (FMCW) radar has been widely studied in these days. The system is used not only for obtaining the range and the velocity of targets, but also for measuring the angular position of the targets. The direction of arrival (DOA) estimation algorithms such as the conventional beamforming (i.e., the Bartlett estimation), the multiple signal classification (MUSIC), the Root-MUSIC, and the estimation of parameters via rotational invariance technique (ESPRIT) have been equipped with the FMCW radar system for determining the angle information

of the desired targets [1]-[3]. These algorithms can be allowed with certain conditions for the number of desired targets, incoherence of received signals reflected from different targets, and the angular location of targets, etc. [4], [5].

When the assumptions on the prior information are satisfied, most of these algorithms show superior performance. However, it is hard to fulfill the assumptions on the prior information in the practical situation. The performance of the MUSIC algorithm, known as the super-resolution DOA estimation algorithm, is even worse than the performance for the more robust conventional DOA estimation algorithm (e.g. the Bartlett estimation). For example, the MUSIC algorithm operates properly when the signals reflected from different targets are incoherent and the number of targets is perfectly known. Since the algorithm is applied for the practical case where the signals could be coherent and the number of targets is veiled, the prior assumption may not be valid for the FMCW radar systems.

To distinguish the closely adjacent targets, DOA estimation algorithms with high angular resolution are required. The angular resolution can be enhanced by extending the aperture size of array and expanding the number of antennas. In this paper, therefore, we propose a virtual antenna generated by the interpolated array technique to increase the angular resolution while maintaining the given aperture size of the array and the number of antennas

[6]-[11]. Since the proposed technique provides an enhanced angular resolution without increasing the aperture size of the array and the number of antennas, it enables to design the compact radar. The performance of the proposed virtual array is almost equivalent to the DOA estimation performance of the large aperture size of the array and the more number of antennas.

3.2 Interpolated Array Technique

Direction-finding techniques based on the eigendecomposition of the covariance matrix of the vector of the signals received by an array of sensors, have received considerable attention in recent years. The main advantage of using techniques such as the multiple signal classification (MUSIC) algorithm [1], rather than a maximum likelihood estimator, is their relative computational simplicity. The MUSIC algorithm involves a one dimensional search, compared with the multidimensional search inherent in the maximum likelihood technique. Certain variants of MUSIC, such as root-MUSIC avoid the search completely (or rather, replace it with a root solving algorithm), reducing even further the computational complexity of the direction finding algorithm.

The idea of an interpolated array is based on estimating the outputs of a "virtual array" from the outputs of the real array. These outputs are obtained by a straightforward linear interpolation technique, with interpolator coefficients selected so as to minimize the interpolation error for a signal arriving from a given sector (i.e., a range of bearing angles). Different sets of interpolator coefficients are used to provide good estimates for different sectors. The size of the sector is chosen to give sufficiently good estimates of the virtual array outputs. The design of the interpolator needs to be performed only once, off-line.

Given measurements of the real array outputs, the interpolator can be used in principle to compute the outputs of the virtual array. (More precisely, several sets of outputs are computed, one per sector.) Any direction finding technique can then be applied to the outputs of the virtual rather than the real array.

I outline the steps involved in designing the interpolated array and discuss various issues related to the array design.

3.2.1 Steps in the Interpolated Array Design

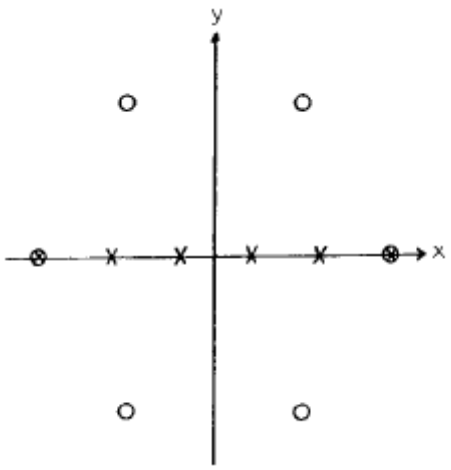

Figure 3.1 The geometry of the UCA and ULA

In array interpolation, the main idea is to find an interpolation matrix which will linearly transform the real array. In this method, the real array manifold is approximated by a virtual array manifold. The following is a step-by-step description of what needs to be done to design the interpolated array [6]-[8].

Step 1. The first step is choosing the field of view of the array. The field of view of the array named Θ is chosen as $[-90^{\circ}, 90^{\circ}]$ or narrower. The field of view will be divided into L sectors. The l-th sector is defined by the interval $[\theta_L, \theta_R]$.

Step 2. Assume there is a signal located in the sector, it is defined as:

$$\Theta = [\theta_L, \theta_L + \Delta\theta, \theta_L + 2\Delta\theta, \cdots, \theta_R - \Delta\theta, \theta_R] \quad (3.1)$$

which is covering each sector ($\Delta\theta$ is the step size). These angles are used only in the design of the interpolation matrix. (The step size is chosen by user selection).

Step 3. Compute the steering vectors associated with the set Θ for the real array and express them in a matrix as follows:

$$\mathbf{A_r} = [a_r(\theta_L), a_r(\theta_L + \Delta\theta), \cdots, a_r(\theta_R)] \quad (3.2)$$

In other words $\mathbf{A_r}$ is section of the array matrix of the real array.

Next, the positions of virtual elements by the interpolated array technique should be decided. The number of virtual array is assumed to be N elements. It is assumed that the virtual array is always uniform linear array (ULA). According to the 'Rule of Thumb', the positions of virtual elements are close to the positions of real element. The aperture size of the virtual array is set to be approximately equal to the aperture size of the real array.

Step 4. Since the decision of element locations of virtual array is finished, the steering vectors associated with the sector can be calculated. We denote by $\mathbf{A_v}$ the section of this steering vector computed for the set of angles Θ :

$$\mathbf{A_v} = [a_v(\theta_L), a_v(\theta_L + \Delta\theta), \cdots, a_v(\theta_R)] \tag{3.3}$$

In other words, $\mathbf{A_r}$ is the steering matrix of the real array to signals arriving from directions Θ, and $\mathbf{A_v}$ is the steering matrix of the virtual array to the same signals.

Step 5. Basic assumption is that the array manifold of the virtual array can be obtained by linear interpolation of the array manifold of the real array in each sector *l.* That is, there exists a constant transformation matrix $\mathbf{T}$ satisfying the equation,

$$\mathbf{A_v} = \mathbf{T}\mathbf{A_r} \tag{3.4}$$

This is an approximate equality. The computation of $\mathbf{T}$ matrix is performed by a least-squares optimization. The optimization interpolation matrix is the one which will give the best fit between the interpolated response $\mathbf{TA_r}$, and the desired response $\mathbf{A_v}$. The optimization solution of $\mathbf{A_v} = \mathbf{TA_r}$ which may be given by

$$\mathbf{T} = \mathbf{A_v}\mathbf{A_r^H}(\mathbf{A_r}\mathbf{A_r^H})^{-1} \tag{3.5}$$

3.3 The Grating Lobe Suppression Scheme

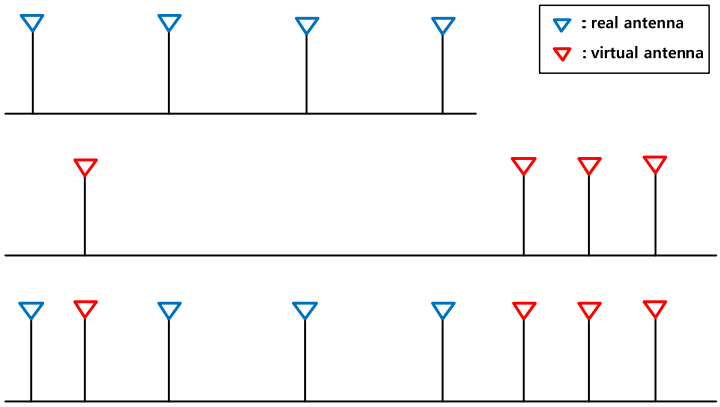

Figure 3.2 Virtually extended array by the proposed technique

If some array has the grating lobe or side lobe comparable to the main lobe, the radar system confronts the problem with an angular resolution. Thus, the grating lobe/side lobe suppression is the important issue to enhance the performance of the radar system. The proposed technique is developed to reduce or suppress the grating lobe/side lobe by virtually extended array with the interpolated array technique [12] and allows distinguishing the closed targets although the targets are not distinguished with the real array. The interpolation technique to change the uniform linear array (ULA) into the non-uniform linear array (NLA) is firstly used to suppress the grating lobe with the expanded number of antennas and to enhance the angular resolution

with the extended aperture size by combining the real array and virtual array. The conventional interpolation technique transforms the uniform array into the different uniform array with new antenna spacing and the original array and the new array which is moved by the conventional method are not used together. There are no researches that the interpolated array technique is applied to the Bartlett algorithm to suppress the grating lobe for the accurate DOA estimation as well as to enhance the angular resolution [5]-[8]. The following is a step-by-step description to be done to design the proposed technique.

Step 1. The locations of the real array for uniformly spaced linear array are $[d_1, d_2, \cdots, d_N]$ and those of the virtual array for non-uniformly spaced linear array are $[d_1', d_2', \cdots, d_M']$, where d_j' $(j = 1, \cdots, M)$ is the location of the j-th element of the virtual array. The followings are constraints for determining the antenna spacing of the real and virtual arrays.

Step 2. We define the sector Θ depending on the field of view (angular range) of the radar system. The transformation matrix $\boldsymbol{T}$ is computed according to the defined sector. To improve the DOA estimation accuracy,

the sector size must be reduced. After the target angle is estimated first, the sector is reduced to the proper angle range including the target angle.

a. $\Theta_1 = [\theta_L, \theta_R] \Rightarrow \Theta_2 = [\theta'_L, \theta'_R]$

b. $\theta_L < \theta'_L,\ \theta_R > \theta'_R,\ \theta'_L < \theta_T < \theta'_R$

where θ_T is the angle of the desired target.

Step 3. For the next step, the received signals of the virtual array are computed as,

$$\mathbf{x}_v = \mathbf{T}\mathbf{x}_r = \mathbf{T}(\mathbf{A}_r\mathbf{s} + \mathbf{n}) = \mathbf{T}\mathbf{A}_r\mathbf{s} + \mathbf{T}\mathbf{n} \simeq \mathbf{A}_v\mathbf{s} + \mathbf{T}\mathbf{n} \quad (3.6)$$

$$\begin{bmatrix} x_{v,1} \\ x_{v,2} \\ \vdots \\ x_{v,\mathrm{M}} \end{bmatrix} = \mathbf{T} \begin{bmatrix} x_{r,1} \\ x_{r,2} \\ \vdots \\ x_{r,N} \end{bmatrix} \quad (3.7)$$

where $x_{r,i}$ is the received signal at the i-th element of the real array and $x_{v,\mathrm{j}}$ is the received signal at the j-th element of the virtual array.

Step 4. Combine the received signals of the virtual and real arrays so that they end up as one array x_T as shown in figure 3.2. Compute the correlation matrix R_T for the received signals of the combined array.

$$\mathbf{x}_T = \begin{bmatrix} \mathbf{x}_r \\ \mathbf{x}_v \end{bmatrix} = \begin{bmatrix} \mathbf{x}_r \\ \mathbf{T}\mathbf{x}_r \end{bmatrix} \tag{3.8}$$

$$\mathbf{R}_T = E[\mathbf{x}_T \mathbf{x}_T{}^H] \tag{3.9}$$

The Bartlett pseudo-spectrum from the virtually extended array is given as,

$$P_{B,T}(\theta) = \frac{\mathbf{a}_T{}^H(\theta)\hat{\mathbf{R}}_T\mathbf{a}_T(\theta)}{\mathbf{a}_T{}^H(\theta)\mathbf{a}_T(\theta)} \tag{3.10}$$

where $\mathbf{a}_T(\theta) = [\mathbf{a}_r(\theta) \quad \mathbf{a}_v(\theta)]^T$.

Step 5. We suggest two conditions to determine the spacing of the virtual array. First, choose the antenna spacing of the virtual array, which has the minimum root mean square error (RMSE) for DOA estimation calculated from the Bartlett pseudo spectrum of the virtually extended array.

$$p_1^{*} = \arg_{p}\left(\min\left(\sqrt{\frac{1}{L}\sum_{l=1}^{L}(\theta_l - \hat{\theta}_{l,p})^2}\right)\right) \tag{3.11}$$

Where $\hat{\theta}_{l,p}$ is the estimated DOA of the l-th target with *p*-th combination of virtual array $[d'_{1,p}, d'_{2,p}, \cdots, d'_{M,p}]$. $d'_{j,p}$ $(j = 1, 2, \ldots, M)$ is the location of j-th element in the p-th combination.

Next, the variables $d'_{j,p}$ for the location of virtual antenna element are selected to minimize the energy of grating lobe and side lobe in the pseudo spectrum of the Bartlett algorithm.

$$p_2^{*} = \arg_{p}\left(\min \ \frac{1}{|\theta_R|}\int_{\theta_R}\left|P_{B,T}(\theta)\right|^2 d\theta - \sum_{l=1}^{L}\left(\frac{1}{|\theta_l|}\int_{\theta_l}\left|P_{B,T}(\theta)\right|^2 d\theta\right)\right) \tag{3.12}$$

The range θ_R of integration is $[-90^{\circ}, 90^{\circ}]$ and the range θ_l is $[\hat{\theta}_l - \frac{1}{2}\hat{\theta}_{l,3dB}, \hat{\theta}_l + \frac{1}{2}\hat{\theta}_{l,3dB}]$, where $\hat{\theta}_l$ is the *l*-th estimated angle of target and

$\hat{\theta}_{l,3dB}$ is the half-power(3dB) angle at the peak corresponding to the *l*-th target in the Bartlett pseudo spectrum.

3.4 Simulation and Measurement Results

3.4.1 Array Design

The grating lobe, which is a lobe with the same height as the main lobe, degrades the DOA performance [13]. The relationship between the angle θ_g at which the first grating lobe appears, and the angle θ_o to which the main beam is steered, is given by [14],

$$\left|\sin\theta_g - \sin\theta_o\right| = \frac{\lambda}{d} \tag{3.13}$$

The grating lobe can be suppressed by adding the new beam pattern formed by the virtual antennas. The specific non-uniform array with the proposed technique is designed to decrease the effect of grating lobe as suppressing the known location of the grating lobe [15]. The antenna spacing and the number of elements for the array design were used like that in the practical radar system that will be introduced in the measurement in section 3.4.3. The number of the antenna elements is four and the spacing between two elements

is 1.8λ. The antenna element positions for a specific non-uniform array are designed within $0.1\lambda \leq d \leq 12.0\lambda$ in steps of 0.1λ. Four elements of virtual array within 0.1λ to 12λ in steps of 0.1λ ([0.1 0.2 0.3 0.4] λ to [11.7 11.8 11.9 12.0] λ) are changed for the exhaustive search. Total 8,214,570 combinations of virtual array are simulated for array design and best one of combinations is chosen. The array with virtual antenna elements has a smaller beamwidth than that of the given real four-elements uniform linear array. Regardless of the target position, the beamwidth of the extended array with virtual array elements is smaller than that of the real uniform array due to the virtually broadened aperture size. The number of virtual antenna elements is constrained to the same number of the real array, M=N. When M>N or M<N, the performance of the proposed technique shows almost same (M>N) or less (M<N) improvement as compared with M=N. As M becomes bigger, the performance is improved in M<N range. And then, when M becomes N (M=N), the performance is saturated. Moreover, the computational complexity for the DOA estimation and array design also exponentially increases for M>N.

\indent The Bartlett algorithm is used to evaluate the performance of the extended array with virtual elements. Table 3.1 shows the numerical values calculated from the section 4 in step 5 for the corresponding the area of

grating lobe and side lobe in the Bartlett spectrum to measure the grating lobe and side lobe level, and maximum angular resolution where d_j' $(j=1,2,3,4)$ is the *j*-th position of virtual antenna, the real array is [0 1.8 3.6 5.4]λ and the target is located at [-3° 4°]. For first step, according to the field of view (FOV) of practical radar specification, the initial sector $[\theta_L, \theta_R]$ is set to $[-15^\circ, 15^\circ]$. In this sector, estimated target direction is roughly found. For next step, another sector $[-5^\circ, 5^\circ]$ where the estimated target direction is included for improving the angular resolution is used. The reason why $[-5^\circ, 5^\circ]$ is used for the second sector is that two targets with 10° or above spacing need not to be considered because two targets are estimated well even if the sector size is not reduced. In first step, the virtual arrays are picked in the top 10% results with first criteria p_1^*. With second criteria p_2^*, the virtual arrays are picked in the top 10% results again. About 80,000 combinations of virtual array are remained. After the sector is reduced to $[-5^\circ, 5^\circ]$, the combinations of virtual array whose RMSE is less than 0.5° is chosen with first criteria p_1^*. Finally, top 5 virtual arrays are chosen with the p_2^*.

	d_1'	d_2'	d_3'	d_4'	Area of GL+SL	Max. AR
1	1.0λ	6.2λ	7.0λ	8.7λ	77.01	6°
2	2.5λ	6.2λ	7.0λ	8.7λ	81.41	6°
3	4.4λ	6.1λ	6.9λ	8.6λ	81.46	6°
4	1.0λ	6.2λ	7.2λ	8.9λ	96.99	6°
5	1.0λ	6.2λ	8.4λ	9.0λ	98.01	6°

(d_j' : j-th position of virtual antenna, AR : angular resolution)

Table 3.1. Area of grating lobe, side lobe and maximum angular resolution via different array with virtual antenna positions

3.4.2 Simulation Results

In this section, we evaluate the performance of the propose technique by analyzing the Bartlett pseudo spectrum. A uniform linear array is considered to have 4 elements for the real array with different antenna spacing. The number of time samples K=2000, SNR=10dB, and step size $\Delta\theta = 0.1$ are used for simulations.

Case 1. Set the location of the real array $[0\ 1.8\ 3.6\ 5.4]\lambda$ that the large antenna spacing makes the sharp beam with the grating lobes, and the location of the virtual array is $[1.0\ 6.2\ 7.0\ 8.7]\lambda$ which is selected from Table 3.1. The virtually extended arrays have the location of $[0\ 1.0\ 1.8\ 3.6\ 5.4\ 6.2\ 7.0\ 8.7]\lambda$ and the target is placed at $[-3^\circ\ 4^\circ]$. Figure 3.3 shows the normalized Bartlett spectrum when the sector is $[-15^\circ, 15^\circ]$.

The virtually extended array with the proposed technique (red line) indicates two peaks for each target. However, the real array (blue line) fails to distinguish between the two targets. In this case, the angle for the two targets is $[-3.3^\circ\ 4.3^\circ]$ where the accuracy of performance is not satisfactory. According to step 2 in section 3.3, the sector needs to be modified to increase the accuracy of performance. The accuracy of DOA estimation is improved even though the side lobe level is slightly increased by adjusting the sector to $[-5^\circ, 5^\circ]$ as shown in figure 3.4. The estimated angle of two targets is $[-2.9^\circ\ 4.1^\circ]$ for the reduced sector.

The estimated angle shows almost the same values as the target angles. The grating lobe level in the virtually extended array is much lower than that in the

real array. As the grating lobes are suppressed, the radar system becomes more stable and reliable.

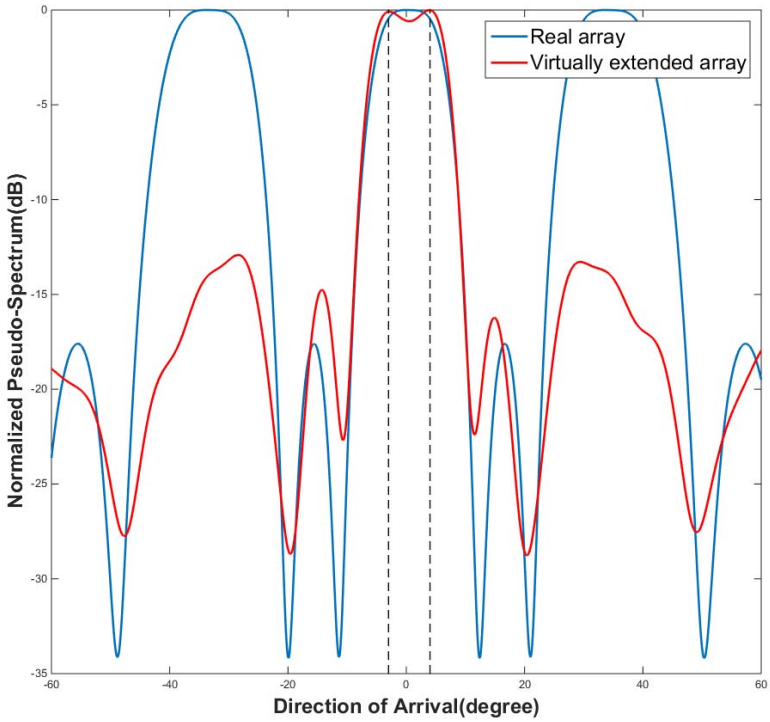

Figure 3.3 Bartlett Pesudo Spectrum for the sector $[-15^{\circ},15^{\circ}]$

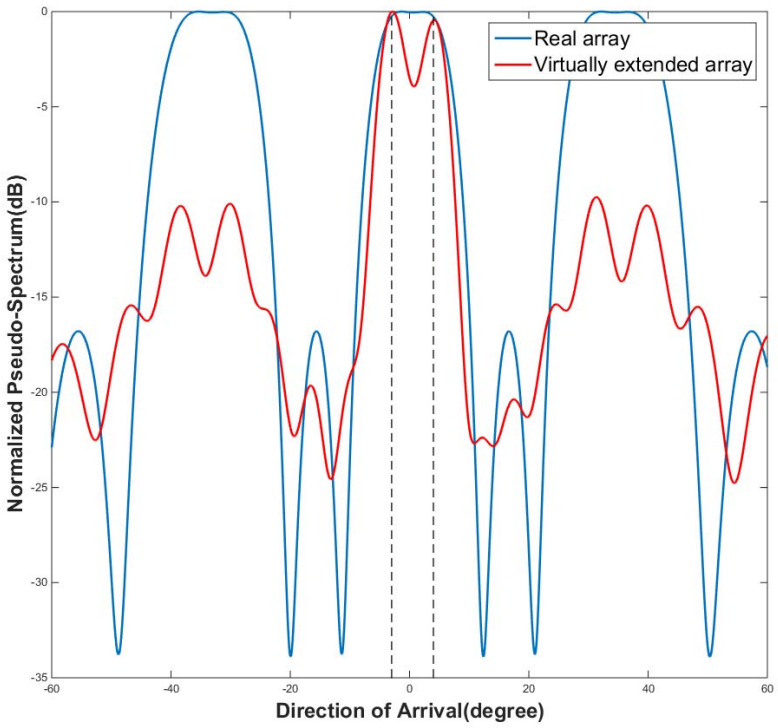

Figure 3.4 Bartlett Pesudo Spectrum for the sector $[-5^{\circ}, 5^{\circ}]$

Case 2. In this case, three different virtually extended arrays are compared with different number of antenna elements with the same aperture size. One array has full virtual antennas and other arrays miss some virtual antennas with the same number of real antennas.

The first array is the same as in case 1 with virtually extended array location at $[0\ 1.0\ 1.8\ 3.6\ 5.4\ 6.2\ 7.0\ 8.7]\lambda$. The second array uses two virtual antennas $[1.0\ 7.0]\lambda$ so that the location of virtually extended array is $[0\ 1.0\ 1.8\ 3.6\ 5.4\ 7.0]\lambda$. The third array uses two virtual antennas $[6.2\ 8.7]\lambda$ so that the location of virtually extended array is $[0\ 1.8\ 3.6\ 5.4\ 6.2\ 8.7]\lambda$.

As shown in figure 3.5, the grating lobes still exist in the second and the third array due to some missing virtual antennas. The estimated angle of desired targets in the first array is $[-2.9^{\circ}\ \ 4.1^{\circ}]$. Although the Bartlett spectrum of the second (blue line) and the third (black line) array indicates two peaks in the center, there still exist significant side lobes to make hard to find the angle of targets in the radar system.

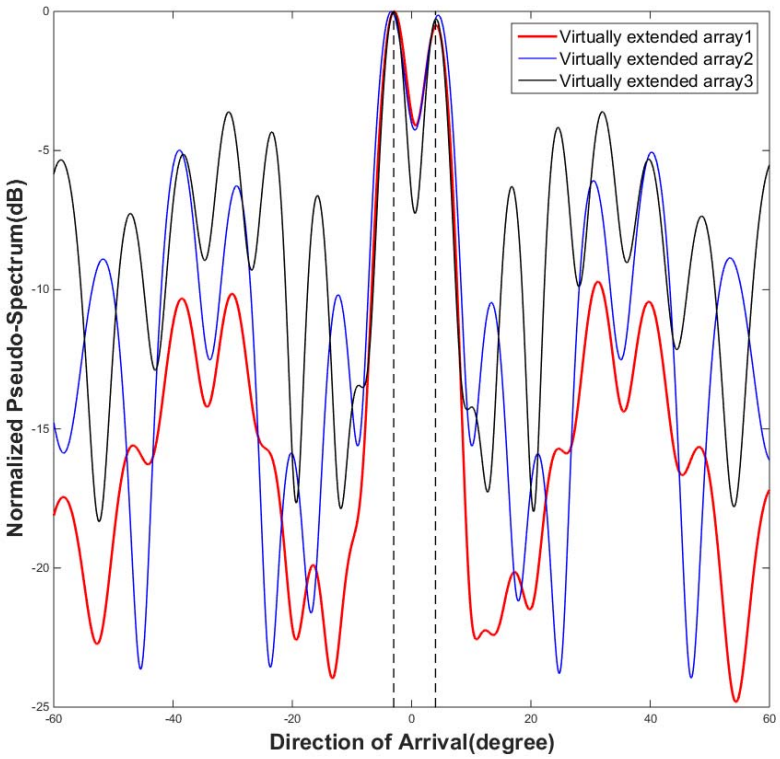

Figure 3.5 Comparison of three different arrays with the sector $[-5^{\circ}, 5^{\circ}]$

Case 3. The conventional interpolated array technique used only virtual antennas. To compare the performance of the conventional technique and the proposed technique, the two arrays which consist of only virtual antennas and virtually extended array are used. The simulation environment is the same as case 2. The location of array with only virtual antennas is $[1.0\ \ 6.2\ \ 7.0\ \ 8.7]\lambda$ and the virtually extended array is $[0\ 1.0\ 1.8\ 3.6\ 5.4\ 6.2\ 7.0\ 8.7]\lambda$.

The peaks of Bartlett spectrum in the virtually extended array are easier to distinguish than in the array with only virtual antennas as shown in figure 3.6. The estimated target angle in the virtually extended array is $[-2.9^\circ\ \ 4.1^\circ]$ and $[-2.5^\circ\ \ 4.3^\circ]$ in the other array.

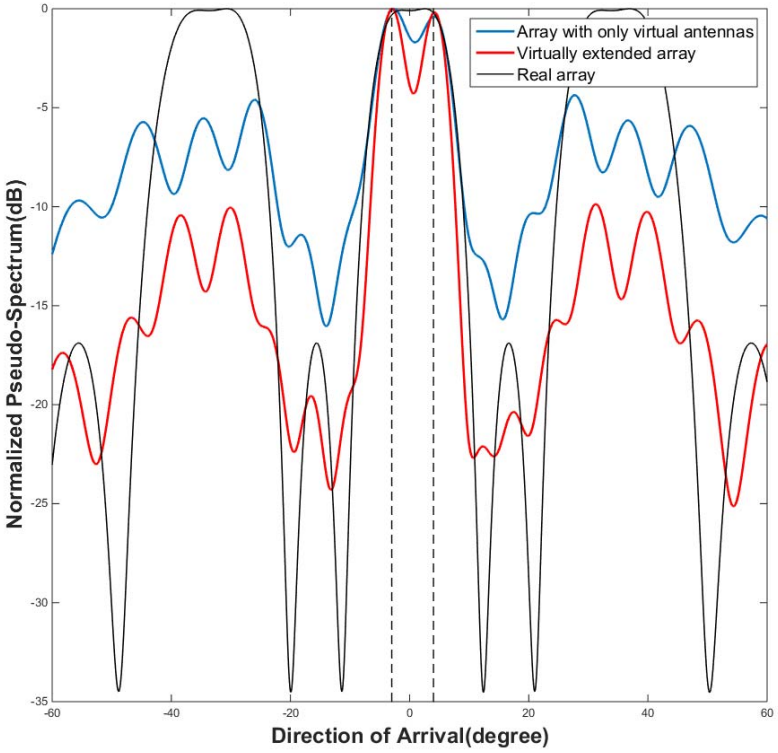

Figure 3.6 Comparison of three different arrays with the sector $[-5^{\circ}, 5^{\circ}]$

Case 4. We analyze the root mean square (RMSE) for DOA estimation via SNR (0dB to 15dB) according to the three array types. The first array is a 12 uniform linear array without virtual antennas. The antenna spacing of the first array is 0.5 λ and the total aperture size is 5.5 λ as the almost same size with the real array [0 1.8 3.6 5.4] λ. The second and third array is the real array and the virtually extended array, which is the same as in case 1. The number of time samples is 2000, 1000 Monte Carlo runs and the angle of targets [-3° 4°] are used.

In Fig. 3.7, the virtually extended array by the proposed technique shows an enhanced RMSE performance than the array without virtual antennas. When the SNR is 10dB, the RMSE of virtually extended array shows 0.7° and the RMSE of real array indicates 2.4°. The accuracy of DOA estimation increases about 1.4° when the virtual antennas are used into the real array.

The RMSE performance for DOA estimation is generally influenced by the SNR. Thus, when the SNR increases, the RMSE performance is improved. Although there are two targets, only one estimated target is found at same direction between two targets for whole SNR range in the case of 12 uniform linear array. As the main beamwidth of 12 ULA is not sharp enough to distinguish the two targets with 7 degree spacing, the RMSE performance of

12 ULA is unchanged regardless of SNR.

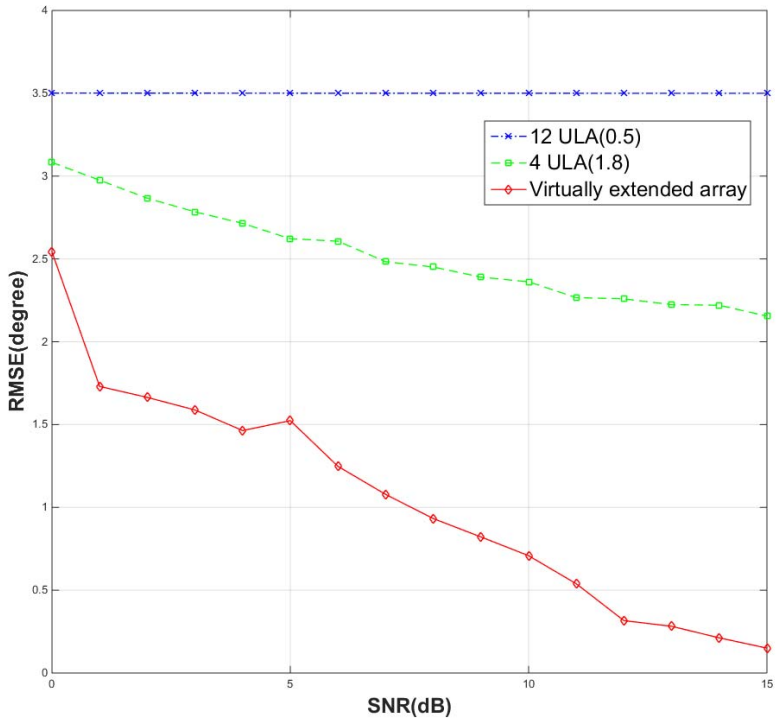

Figure 3.7 RMSE via SNR for four types of array

3.4.3 Experimental Results

Figure 3.8 Photograph of the experiment environment

To verify the performance of proposed technique in the various scenarios, a measurement was carried out. To avoid extraneous effects from clutters like traffic signs, the road measurement was carried out in a huge empty space. The 76.5GHz FMCW radar system, a sweep bandwidth and a sweep time is 500MHz and 5ms, is used. The dynamic range is 250m and the field of view (angular range) is $\pm 10^{\circ}$. There are two stationary cars at 40m where the spacing between the targets is 3.6m, as shown in figure 3.8. The angle of

targets is located at $[-3^\circ\ 3^\circ]$ and the practical antenna spacing of the real array is $[0\ 1.8\ 3.6\ 5.4]\lambda$.

The angle of two targets is analyzed with the proposed technique and conventional interpolation array technique from the experimental data. The first analysis used the virtual array $[1.0\ 6.2\ 7.0\ 8.7]\lambda$ to make the virtually extended array and the array with only virtual antennas for conventional technique. The estimated angle of the desired target is $[-3^\circ\ 3.5^\circ]$ by the proposed technique (red line) and $[-4.1^\circ\ 4^\circ]$ by the conventional interpolation array technique (blue line), as seen in figure 3.9. When the array with only virtual antennas is used, the significant side lobes are observed. The desired targets cannot be distinguished when the real array is only used to estimate the angle of targets.

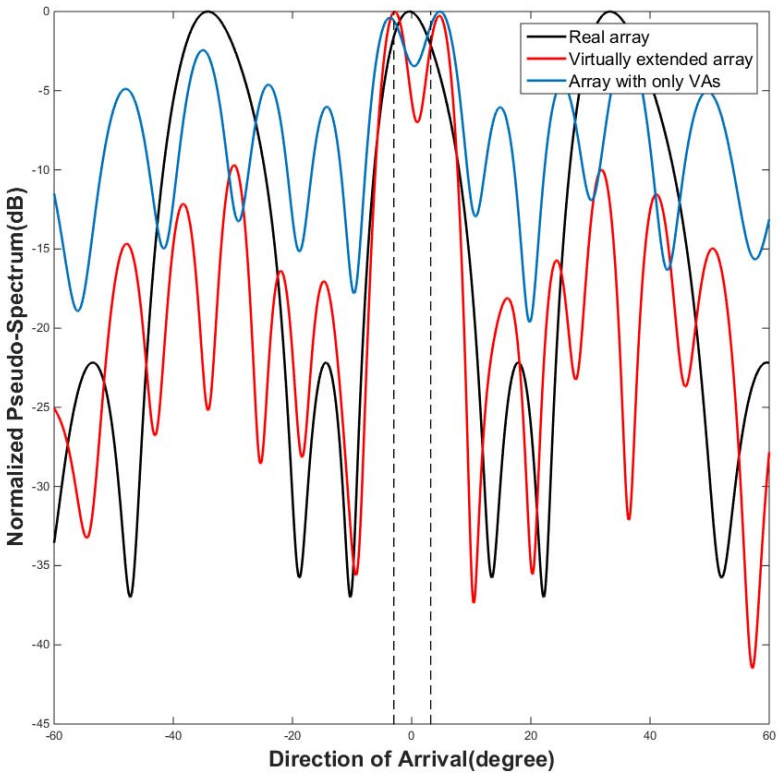

Figure 3.9. DOA analysis of the experiment with the sector $[-5^{\circ}, 5^{\circ}]$

The MUSIC algorithm is used to compare with the performance of the proposed technique. The grating lobes make hard to find the actual target angle as shown is figure 3.10. The estimated angle at the center of spectrum is $[-1.9^{\circ}\ 4.6^{\circ}]$. The estimated angles of error are -1.1 and 1.6 for the left and right targets with the MUSIC algorithm. The errors for the left and right targets are 0.2 and 1.4 with the proposed technique. The proposed technique shows the more accurate angular resolution than the MUSIC algorithm and has no grating lobes.

The signal strength varies according to the incoming direction because two signals are passed through the two different channels and reflected from different targets. For that reason, the peak of two signals showed different level in the spectrum of simulation and experimental results.

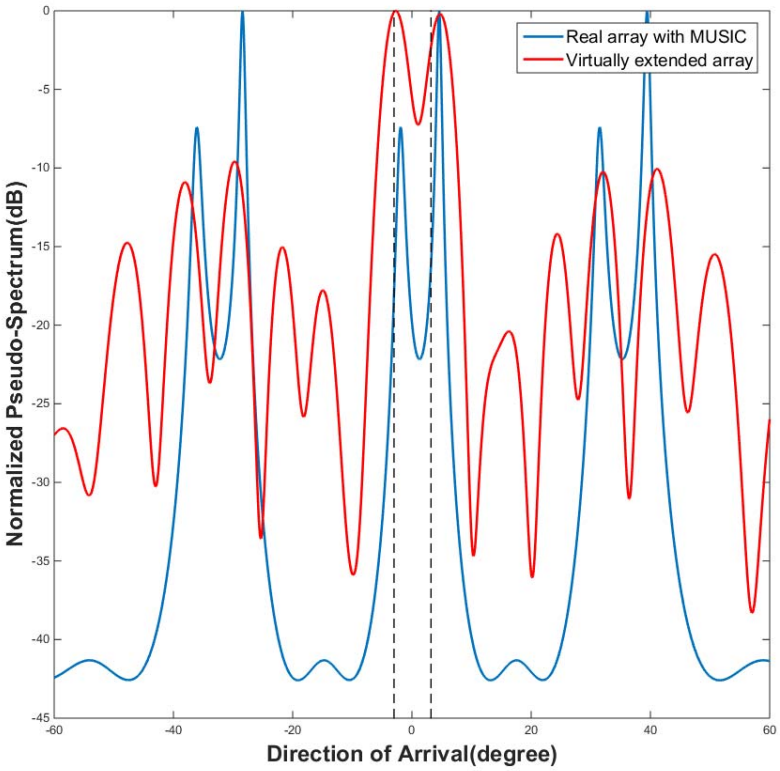

Figure 3.10. DOA analysis of experiment with MUSIC algorithm

Chapter 4. The Signal Power Compensation Technique

4.1 Introduction

The radiation beam pattern of an antenna array depends strongly on the weighting method and the geometry of the array. Selection of the weights has received extensive attention, primarily because the radiation pattern is a linear function of the weights. However, the array geometry has received relatively little attention even though it also strongly influences the radiation pattern. The reason for this is primarily due to the complex way in which the geometry affects the radiation pattern. The virtual antenna technique with the goal of suppressing grating lobe and improving angular resolution is investigated. The main purpose of this chapter is to determine weights of improving the performance in virtually extended array.

Grating lobe and side lobe level is an important factor to estimate the angle of targets in antenna arrays, and depends on the weights and positions in the array.

4.2 The Limitation of Array Interpolation

In array interpolation, a transformation matrix **T** is used to obtain data from a virtual array when the data from an actual array is given. In order to have an accurate mapping (or interpolation), the number of actual sensors is usually selected larger than the virtual array elements [6].

Furthermore mapping is devised only for an angular sector $[\theta_L, \theta_R]$ where the sources are assumed to be located. Let $\mathbf{A_v}$ and $\mathbf{A_r}$ be the steering matrices for the angles in the angular sector for the virtual array and real array respectively. N by M transformation matrix designed for the best square fit between range spaces of these two steering matrix matrices is,

$$\mathbf{T} = \mathbf{A_v}\mathbf{A_r^+} = \mathbf{A_v}\mathbf{A_r^H}(\mathbf{A_r}\mathbf{A_r^H})^{-1}$$

where $\mathbf{A_r^+}$ is the Moore-Penrose pseudo-inverse. Both $\mathbf{A_v}$ and $\mathbf{A_r}$ are built by dividing the angular sector $[\theta_L, \theta_R]$ into $\Delta\theta$ intervals. Since transformation matrix **T** is found as the least squares solution, as the $\theta_R - \theta_L$ increases, the accuracy of the mapping decreases. On the other hand, there is no information regarding the source direction a priory and it is desired to keep $\theta_R - \theta_L$ as large as possible to cover the most of the looking directions. This contradiction is one of the limitations of array interpolation. Another problem

in finding **T** is the condition number of $\mathbf{A}_r\mathbf{A}_r^H$. This matrix may be ill-conditioned for certain angular sectors [6].

4.3 The Signal Power Compensation Technique

There are some combinations of virtual array which are not satisfied with the valuation criteria 1, 2 from the section 3.3, step 5. As I already mentioned about the calculation error of transformation matrix **T** in the section 4.2, T includes the error from the calculation of least square method. That error occurs that the data of virtual array, which is made by the transformation matrix with the data of real array, is not perfectly realized. Then, the data of some virtual array shows lack of the signal power. For example, the virtual array $[4.3\ 4.9\ 11.3\ 11.9]\lambda$ shows the good performance in terms of angular resolution. However, this combination of virtual array is not selected by the criteria 2 which include the area of grating lobe and side lobe. The data of virtually extended array with this combination is obtained with two targets $[-3^\circ\ 4^\circ]$, sector $[-5^\circ,5^\circ]$, and number of time sample 2000. The received signal strength and correlation matrix are calculated as,

$$|\mathbf{X}_T| = \begin{bmatrix} 2591.849 \\ 2633.86 \\ 2622.856 \\ 2581.807 \\ 2713.728 \\ 2743.443 \\ 32.51288 \\ 211.6 \end{bmatrix}$$

Figure 4.1 Strength of received signal before applying power compensation

$$|\mathbf{R}_T| = \begin{bmatrix} 2.062 & 1.566 & 0.423 & 0.922 & 0.193 & 0.675 & 0.010 & 0.123 \\ 1.566 & 2.104 & 1.593 & 0.404 & 1.170 & 0.742 & 0.014 & 0.027 \\ 0.423 & 1.593 & 2.111 & 1.553 & 2.079 & 1.872 & 0.020 & 0.070 \\ 0.922 & 0.404 & 1.553 & 2.046 & 1.963 & 2.144 & 0.018 & 0.151 \\ 0.193 & 1.170 & 2.079 & 1.963 & 2.263 & 2.217 & 0.021 & 0.115 \\ 0.675 & 0.742 & 1.872 & 2.144 & 2.217 & 2.315 & 0.021 & 0.145 \\ 0.010 & 0.014 & 0.020 & 0.018 & 0.021 & 0.021 & 0.001 & 0.001 \\ 0.123 & 0.027 & 0.070 & 0.151 & 0.115 & 0.145 & 0.002 & 0.013 \end{bmatrix}$$

Figure 4.1 Correlation matrix before applying power compensation

As shown in figure 4.1, the signal strength of 7,8th antennas shows relatively much smaller than the strength of other antennas. This means that there are almost no influences of 7,8th antenna. In the correlation matrix, the diagonal elements refer to the power of each antenna.

To compensate the signal strength of 7,8th antennas, I multiply the weighting

factor to those of antennas. The weighting factor is calculated to adjust the strength of 7,8th antenna with the strength of other antennas. After applying the signal power compensation, the strength of 7,8th antennas is changed similarly with the strength of other antennas as shown in the figure 4.3

$$\left|\mathbf{X}_T^{\mathbf{new}}\right| = \begin{bmatrix} 2591.849 \\ 2633.86 \\ 2622.856 \\ 2581.807 \\ 2713.728 \\ 2743.443 \\ 2607.592 \\ 2607.592 \end{bmatrix}$$

Figure 4.3 Strength of received signal after applying power compensation

$$\left|\mathbf{R}_T^{\mathbf{new}}\right| = \begin{bmatrix} 2.062 & 1.566 & 0.423 & 0.922 & 0.193 & 0.675 & 0.806 & 1.519 \\ 1.566 & 2.104 & 1.593 & 0.404 & 1.170 & 0.742 & 1.187 & 0.336 \\ 0.423 & 1.593 & 2.111 & 1.553 & 2.079 & 1.872 & 1.624 & 0.865 \\ 0.922 & 0.404 & 1.553 & 2.046 & 1.963 & 2.144 & 1.478 & 1.863 \\ 0.193 & 1.170 & 2.079 & 1.963 & 2.263 & 2.217 & 1.756 & 1.418 \\ 0.675 & 0.742 & 1.872 & 2.144 & 2.217 & 2.315 & 1.697 & 1.793 \\ 0.806 & 1.187 & 1.624 & 1.478 & 1.756 & 1.697 & 1.960 & 0.998 \\ 1.519 & 0.336 & 0.865 & 1.863 & 1.418 & 1.793 & 0.998 & 2.086 \end{bmatrix}$$

Figure 4.4 Correlation matrix after applying power compensation

4.4 Simulation Results

Case 1. Set the location of the real array $[0\ 1.8\ 3.6\ 5.4]\lambda$ that the large antenna spacing makes the sharp beam with the grating lobes, and the location of the virtual array is $[4.3\ 4.9\ 11.3\ 11.9]\lambda$. The virtually extended arrays have the location of $[0\ 1.8\ 3.6\ 4.3\ 4.9\ 5.4\ 11.3\ 11.9]\lambda$ and the target is placed at $[-3^\circ\ 4^\circ]$ with the sector $[-15^\circ, 15^\circ]$.

The signal power compensated array (black line) clearly indicates two peaks for each target as shown in the figure 4.5. However, the virtually extended array without signal power compensation technique (red line) fails to distinguish between the two targets.

Case 2. Set the location of the real array $[0\ 1.8\ 3.6\ 5.4]\lambda$ that the large antenna spacing makes the sharp beam with the grating lobes, and the location of the virtual array is $[4.3\ 4.9\ 11.3\ 11.9]\lambda$. The virtually extended arrays have the location of $[0\ 1.8\ 3.6\ 4.3\ 4.9\ 5.4\ 11.3\ 11.9]\lambda$ and the target is placed at $[-3^\circ\ 4^\circ]$ with the sector $[-5^\circ, 5^\circ]$.

The signal power compensated array (black line) and the virtually extended array without signal power compensation technique (red line) clearly indicates two peaks for each target as shown in the figure 4.6. However, the virtually extended array without signal power compensation technique has the more side lobe area than the compensated array.

Case 3. Set the location of the real array $[0\ 1.8\ 3.6\ 5.4]\lambda$ that the large antenna spacing makes the sharp beam with the grating lobes, and the location of the virtual array is $[4.3\ 4.9\ 11.3\ 11.9]\lambda$. The virtually extended arrays have the location of $[0\ 1.8\ 3.6\ 4.3\ 4.9\ 5.4\ 11.3\ 11.9]\lambda$ and the target is placed at $[-3^\circ\ 2^\circ]$ with the sector $[-15^\circ, 15^\circ]$.

The signal power compensated array (black line) clearly indicates two peaks for each target. However, the real array (red line) fails to distinguish between the two targets as shown in the figure 4.7.

The reason why the performance increased is the change in beam pattern of array. Before applying the signal power compensation, the beam pattern of virtually extended array is shown in the figure 4.8. After applying the signal

power compensation, the beam pattern is shown in the figure 4.9. As comparing two beam pattern of figure 4.8, 4.9, the beam pattern which is applied the signal power compensation shows high angular resolution than the beam pattern not applied technique. According to the change of beam pattern, the performance is enhanced in terms of angular resolution and grating lobe/side lobe.

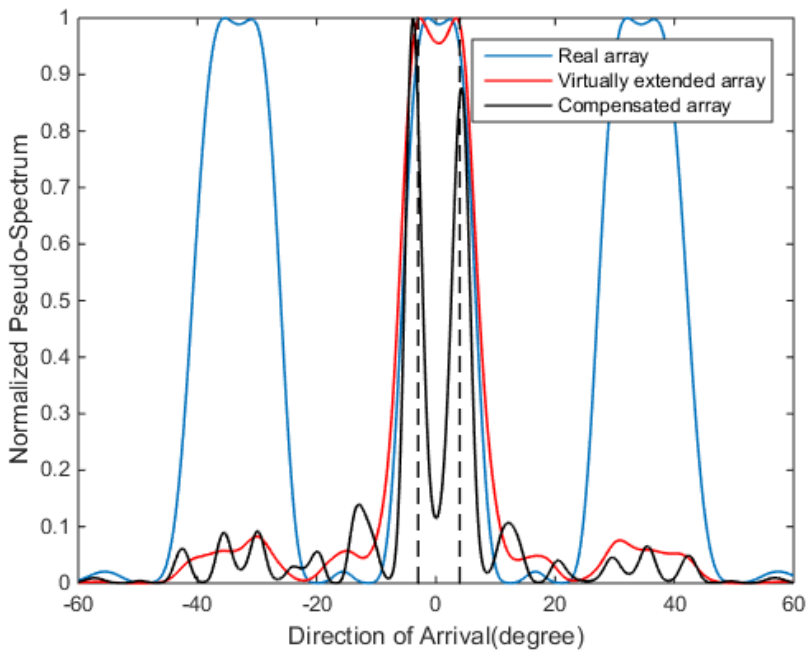

Figure 4.5 Bartlett Spectrum for the sector $[-15^{\circ},15^{\circ}]$, target $[-3^{\circ}\ 4^{\circ}]$

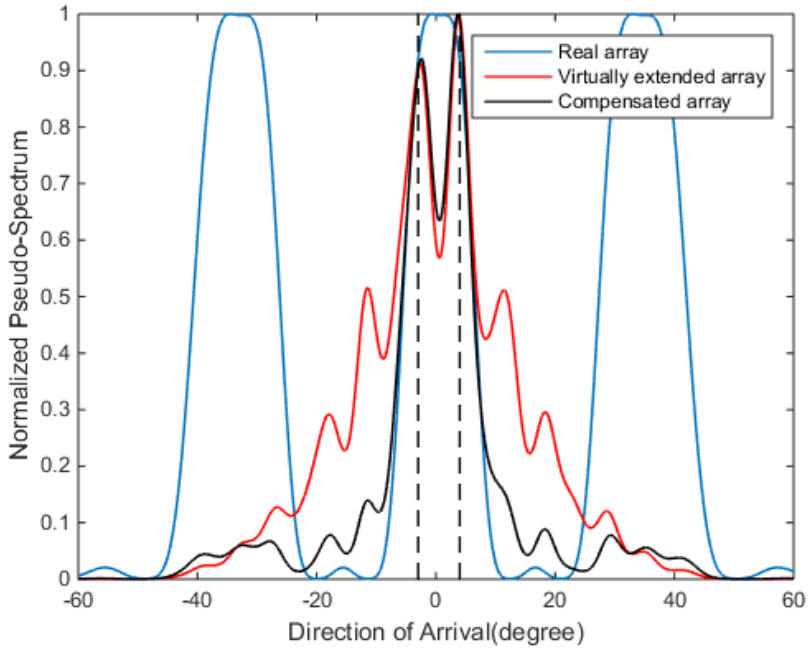

Figure 4.6 Bartlett Spectrum for the sector $[-5^{\circ}, 5^{\circ}]$, target $[-3^{\circ}\ 4^{\circ}]$

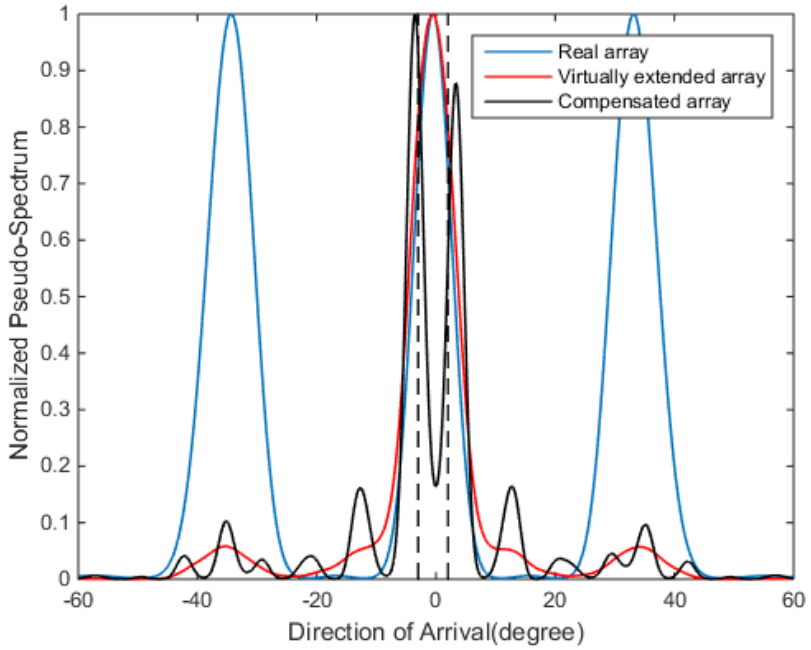

Figure 4.7 Bartlett Spectrum for the sector $[-15^{\circ},15^{\circ}]$, target $[-3^{\circ}\ 2^{\circ}]$

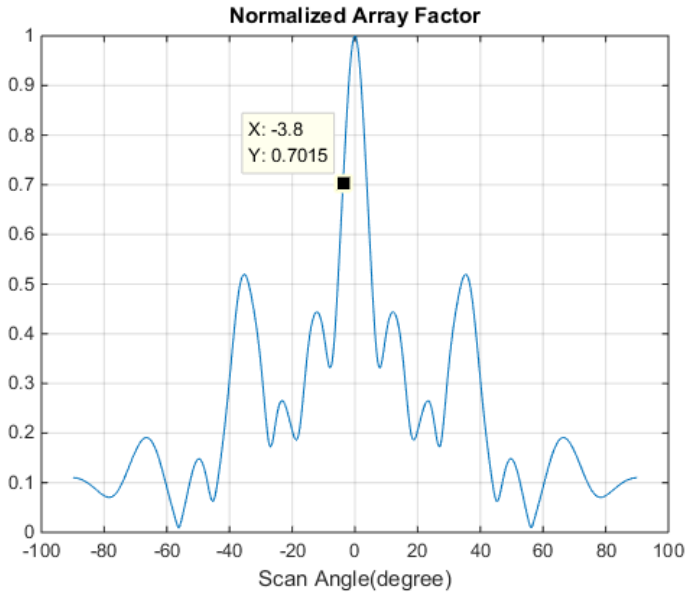

Figure 4.8 Beam pattern before applying signal power compensation

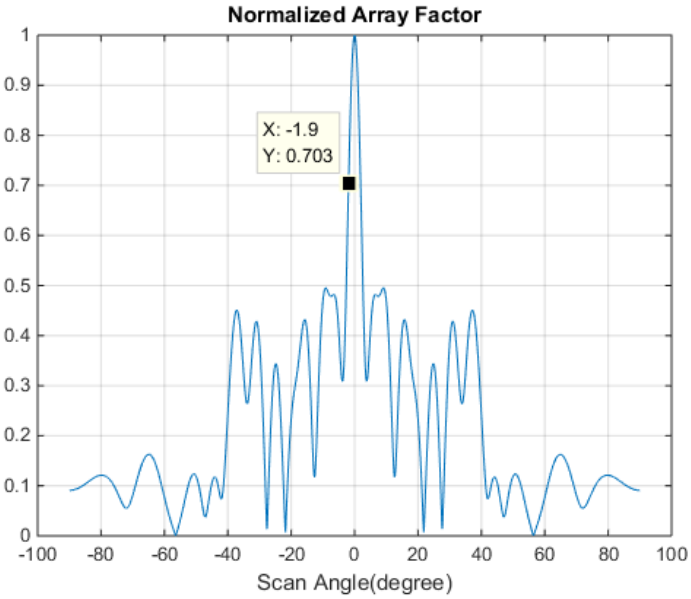

Figure 4.9 Beam pattern after applying signal power compensation

Chapter 5. Conclusion

I presented a new interpolated array technique for a virtually extended array which contains real and virtual antennas. The performance of the Bartlett algorithm is influenced by the number of antennas and the aperture size of the array to make a sharp main beam and suppress the grating and side lobes. The proposed technique provides the virtual extension of number of antennas and aperture size of array without any additional radar production cost. The performance of Bartlett algorithm applied to the proposed technique is analyzed using various simulation environments. The simulation results show that the virtually extended array by the proposed technique enhances the angular resolution of the Bartlett algorithm and has a better DOA estimation accuracy compared to other types of arrays. The proposed technique can be applied to the practical system as verified from practical experiment analysis. Moreover, I proposed the signal power compensation technique to improve the performance of the grating lobe suppression technique. According to the compensation of signal power of antenna which shows relatively weaker than other antennas, the beam pattern (array

factor) is changed to enhance the performance. Therefore, the signal power compensation technique can overcome the limitations of traditional interpolated array techniques. This technique is also analyzed to show the performance improved in the simulations.

Bibliography

[1] H. Krim, M. Viberg, “Two Decades of Array Signal Processing Research: The Parametric Approach”, *IEEE Signal Processing Magazine*, vol.13(4), pp. 67-94, 1996.

[2] L.C. Godara, “Smart Antennas”, *CRC Press*, New York, 2004.

[3] F.B. Gross, “Smart Antennas for Wireless Communications with MATLAB”, *McGraw-Hill*, New York, 2005.

[4] R. Feger, C. Wagner, S. Schuster, S. Scheiblhofer, H. Jager, A. Stelzer, “A 77-GHz FMCW MIMO Radar Based on an SiGe Single-Chip Transceiver”, *IEEE Transaction on Microwave Theory and Techniques*, vol.57(5), pp.1020-1035, 2009.

[5] T.J. Shan, M. Wax, and T. Kailath, “On Spatial Smoothing for Direction of Arrivals Estimation of Coherent Signals”, *IEEE Transaction on Acoustic, Speech, and Signal Processing*, vol.33(4), pp.806-811, 1985.

[6] B. Friedlander, A.J. Weiss, “Direction Finding using Spatial Smoothing with Interpolated Arrays”, *IEEE Transaction on Aerospace Electronic System*, vol.28(2), pp.574-587, 1992.

[7] B. Friedlander, “The Root-Music Algorithm for Direction Finding with Interpolated Arrays”, *Elsevier Signal Processing Journal*, vol.30(1), pp.15-29,

1993.

[8] T.E. Tuncer, T.K. Yasar, B. Friedlander, “Direction of Arrival Estimation for Nonuniform Linear Arrays by using Array Interpolation”, *Radio Science*, vol.42(4) , 2007.

[9] S. Kawakami, O Tomoaki, “Localization using Iterative Angle of Arrival Method Sharing Snapshots of Coherent Subarrays”, *EURASIP Journal on Advances in Signal Processing*, 2011.

[10] W.Q. Wang, “Virtual Antenna Array Analysis for MIMO Synthetic Aperture Radars”, *International Journal of Antennas and Propagation*, vol.2012, 2012

[11] Y.S. Kim, Y.S. Kim, “Improved Resolution Capability via Virtual Expansion of array”, *Electronics Letter*, vol.35(19), pp.1596-1597, 1999.

[12] G. Doblinger, “Optimized Design of Interpolated Array and Sparse Array Wideband Beamformers”, *16th European Signal Processing Conference (EUSIPCO 2008)*, Lausanne, Switzerland, August 25-29. 2008.

[13] S.J. Orfanidis, “Electromagnetic Waves and Antennas”, http://www.ece.rutgers.edu/~orfanidi/ewa

[14] M.I. Skolnik, “Introduction to Radar Systems”, *McGraw-Hill*, New York, 2001.

[15] H. Oraizi, M. Fallahpour, “Nonuniformly Spaced Linear Array Design

for The Specified Beamwidth/Sidelobe Level or Specified Directivity/Sidelobe Level with Coupling Considerations", *Progress in Electromagnetics Research M*, vol.4, pp.185-209, 2008.

[16] T.B. Lavate., V.K. Kokate, and A.M. Sapkal, "Performance Analysis of MUSIC and ESPRIT DOA Estimation Algorithms for Adaptive Array Smart Antenna in Mobile Communication", *International Journal of Computer Netwoks(IJCN)* , 2010.

[17] M. Schoor and B. Yang, "SUBSPACE BASED DOA ESTIMATION IN THE PRESENCE OF CORRELATED SIGNALS AND MODEL ERRORS." *ICASSP*, pp.2161-164, 2009.

[18] P. Häcker, and B. Yang, "Single Snapshot DOA Estimation", *Advances in Radio Science* , pp.251-256, 2010.

[19] T.S. Dhope, D. Simunic, and M. Djurek, "Application of DOA Estimation Algorithms in Smart Antennas Systems", *Studies in Informatics and Control*, ISSN 1220-1766, vol.19(4), pp.445-452, 2010.

[20] M. Schoor and B. Yang, "High-Resolution Angle Estimation for an Automotive FMCW Radar Sensor", *International Radar Symposium, IRS* , 2007.

[21] C.L. Dolph, “A Current Distribution for Broadside Arrays Which optimizes the Relationship between Beam Width and Side-Lobe Level”, *Proceeding of the IRE*, vol. 24(4), pp. 335-348, June 1946.

[22] A. Camps, A. Cardama, and D. Infantes, “Synthesis of Large Low-Redundancy Linear Arrays”, *IEEE Transactions on Antennas and Propagation*, vol. 49 (12), pp. 1881-1883, Dec. 2001.

[23] A. Moffet, “Minimum Redundancy Linear Arrays”, *IEEE Transactions on Antennas and Propagation*, vol. 16 (2), pp. 172-175, Mar. 1968.

[24] P. Hyberg, M. Jansson, “Array Interpolation and Bias Reduction”, *IEEE Transactions on Signal Processing,* vol. 52 (10), pp. 2711-2720, Oct. 2004.

[25] B. Lau, M. Viberg, and Y. Leung, “Data-Adaptive Array Interpolation for DOA Estimation in Correlated Signal Environments”, *IEEE international conference on Acoustics, Speech, and Signal Processing 2005 (ICASSP '05)*, Mar. 2005.

[26] P. Jarske, T. Saramaki, and S.K. Mitra, “On Properties and Design of Nonuniformly Spaced Linear Arrays”, *IEEE Transactions on Acoustics, Speech, and Signal Processing,* vol. 36 (3), pp. 372-380, Mar. 1988.

[27] D.N. Swingler, RS Walker, “Line Array Beamforming using Linear Prediction for Aperture Interpolation and Extrapolation”, *IEEE Transactions on Acoustics, Speech, and Signal Processing,* vol. 37 (1), pp. 16-30, Jan. 1989.

[28] W. Li, X. Mao, W. Yu, and C. Yue, “An Effective Technique for Enhancing Direction Finding Performance of Virtual Arrays”, *International Journal of Antenna Propagation*, vol. 2014, Dec. 2014.

[29] V.R. Lakshmi, G.S.N. Raju, “Optimization of Radiation Patterns of Array Antennas”, *World Conference on Complex Systems (WCCS),* Mar. 2015.

[30] C.E. Kassis, J. Picheral, and C. Mokbel, “Advantages of Nonuniform Arrays using Root-MUSIC”, Elsevier Signal Processing Journal, vol. 90 (2), pp. 689-695, Feb. 2010.

[31] R.W. Bickmore, “Adaptive Antenna Arrays”, *IEEE Spectrum*, vol. 1 (8), pp. 78-88, Aug. 1964.

[32] H. Lebret, S Boyd, “Antenna Array Pattern Synthesis via Convex Optimization”, *IEEE Transactions on Signal Processing*, vol.45(3), pp.526-532, Mar. 1997.

[33] S.P. Applebaum, “Adaptive Arrays”, *IEEE Transactions on Antennas and Propagation,* vol.24(5), pp.585-598, Sep.1976.

[34] M. Rubsamen, A.B. Gershman, “Direction of Arrival Estimation for Nonuniform Sensor Arrays : From Manifold Separation to Fourier Domain MUSIC Methods”, *IEEE Transaction on Signal Processing,* vol.57(2), pp.588-599, Feb. 2009.

[35] X. Zhao, Q. Yang, and Y. Zhang, “Compressed Sensing Approach for Pattern Synthesis of Maximally Sparse Non-Uniform Linear Array”, IET Microwave, Antennas & Propagation, vol.8(5), pp.301-307, Oct. 2013.

[36] P.Y. Zhou, M.A. Ingram, “ Pattern Synthesis for Arbitrary Arrays using an Adaptive Array Method”, *IEEE Transactions on Antennas and Propagation*, vol.47(5), pp.862-869, May 1999.

초 록

요즘에는 운전자가 안전성 확보를 차량에 사용되는 기술 중에서 가장 중요한 문제로 간주한다. 이 사실은 자동차 주변의 상황에 대한 운전자와 차량의 인지도를 높이는데 도움이 되는 몇 가지 유형의 센서들의 개발로 이어졌다. 이러한 차량용 센서로는 카메라, 초음파 및 레이더 센서가 있다. 이러한 센서 중에서 레이더 센서는 다양한 환경 조건에서의 신뢰성 때문에 가장 널리 사용되고 있다. 77 GHz의 FMCW 레이더는 지구상의 환경에 대한 고려의 이유로 널리 연구되고 있다. 이전의 차량용 레이더 시스템은 관찰자와 표적 사이의 거리와 속도의 정보 같은 간단한 정보만을 얻을 수 있었다. 그러나 운전자가 안전에 대한 인식을 더욱 중요하게 생각하게 되어 자동차에서 레이더 시스템의 사용이 급격히 증가하였다.

DOA 추정 알고리즘은 디지털 빔포밍 기술을 사용하여 우리가 원하는 타겟의 정보를 결정하는 중요한 요소를 얻는데 중요한 역할을 하는 알고리즘으로서 인식되고 있다. 고해상도 DOA 추정 알고리즘인 MUSIC, Root-MUSIC 및 ESPIRIT은 매우 인접한 개체를 구별하는 데 사용되고 있다. 이러한 알고리즘을 통해 지연 시간, 주파수, 각도에 대한 정보를 얻을 수 있다. 최근에 이러한

알고리즘은 실제로 사용되는 차량용 레이더의 기능을 향상시키기 위한 적용분야에 대해 연구되고 있다. DOA 추정 알고리즘으로부터 얻어진 각도 정보는 신호들 간의 간섭의 제거 및 원하지 않는 객체들로 인한 클러스터의 제거와 같은 다양한 분야에 적용되고 있다.

이 논문에서 가상 안테나 기법은 도래각(DOA) 추정을 위한 conventional beamforming 기법의 성능을 향상시키기 단일 입력 다중 출력 (SIMO) 레이더 시스템에 적용되었다. 보간된 어레이 기술에 의해 생성된 가상 어레이와 실제 어레이를 결합함으로써, 확장된 안테나 수 및 어레이 개구 크기로 인해 DOA 추정 알고리즘의 각도 분해능이 개선된다. 제안된 보간 기법을 기반으로 균일한 선형배열 (ULA) 에서 안테나 요소의 위치를 임의의 위치로 변환하여 grating lobe와 side lobe 레벨을 억제하거나 줄이는 효과를 얻을 수 있다. 시뮬레이션에서 실제 어레이와 가상적으로 확장된 어레이에 대해 Bartlett 알고리즘의 스펙트럼과 신호 대 잡음비 (SNR)에 따라 DOA 추정의 RMSE (root mean square error)를 분석하였다. 시뮬레이션 결과는 제안된 가상적으로 확장된 어레이의 각도 분해능이 동일한 어레이 개구 크기와 안테나 수를 사용하는 실제 어레이의 각도 분해능보다 우수함을 보여주고 있다. 이 논문에서 제안된 기법은 실제 실험데이터로 분석하여 성능을

검증함에 따라 제안된 기법이 실제 상황에서도 사용될 수 있음을 확인하였다.

주요어 : FMCW, 차량용 레이더, 도래각, 배열 보간법, 가상 안테나
학　　번 : 2010 – 23241